Journal of Sensors

Sensors and Data Processing Techniques for Future Medicine

Lead Guest Editor: Takemi Matsui
Guest Editors: Satoshi Suzuki, Guanghao Sun, and Eddie Ng Yin Kwee

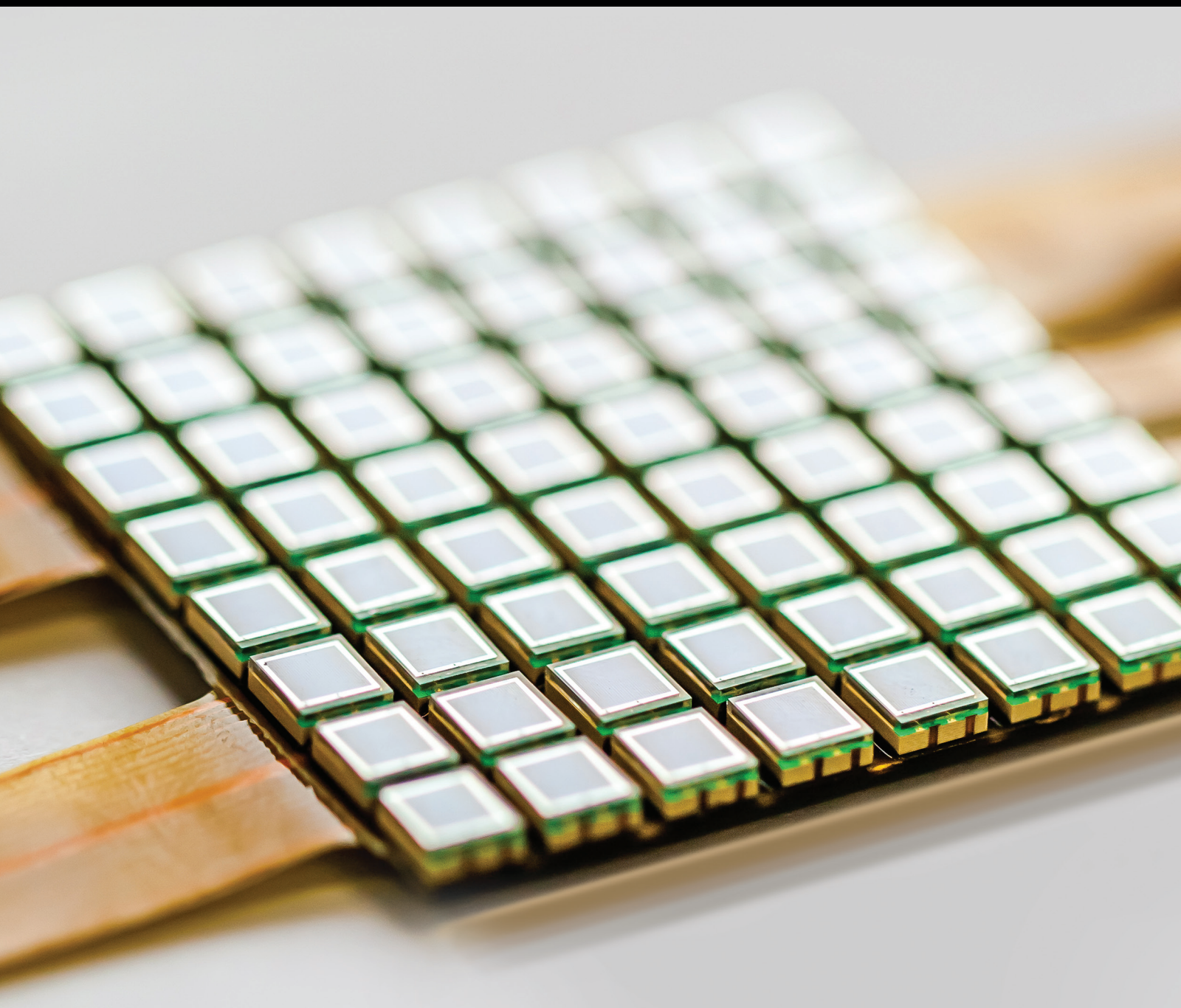

Sensors and Data Processing Techniques for Future Medicine

Journal of Sensors

Sensors and Data Processing Techniques for Future Medicine

Lead Guest Editor: Takemi Matsui
Guest Editors: Satoshi Suzuki, Guanghao Sun, and Eddie Ng Yin Kwee

Editorial Board

Contents

Hindawi
Journal of Sensors
Volume 2018, Article ID 1210609, 2 pages
https://doi.org/10.1155/2018/1210609

Editorial

Sensors and Data Processing Techniques for Future Medicine

Takemi Matsui,[1] **Satoshi Suzuki**,[2] **Guanghao Sun**,[3] **and Eddie Ng Yin Kwee**[4]

[1]*Tokyo Metropolitan University, Tokyo, Japan*
[2]*Kansai University, Osaka, Japan*
[3]*University of Electro-Communications, Tokyo, Japan*
[4]*Nanyang Technological University, Singapore*

Correspondence should be addressed to Takemi Matsui; tmatsui@tmu.ac.jp

Received 29 July 2018; Accepted 29 July 2018; Published 24 September 2018

Varieties of innovative and high precision sensors have been developed and became available for versatile application. Such sensors, when combined with data processing techniques of artificial intelligence, can make a huge impact on healthcare technologies. That is, a system can screen symptoms such as infection, cardiovascular failure, and major depressive disorders, just as experienced physicians diagnose with stethoscope and percussion.

These sensors not only substitute a portion of an experienced physician but also win advantage over physicians in some aspects. A microwave radiated from a small and low-cost microwave-Doppler sensor can penetrate clothes and comforters and monitor not only thoracic respiratory motions and heart rates of patient but also activation of his/her autonomic nerve system located in the hypothalamus of the brain stem using heart rate variability indices calculated from time series of heart rates. An approach has been already conducted to distinguish major depressive disorder patients from normal people under mental work load using a high precision photoplethysmographic sensor, a microwave-Doppler sensor, and a conventional electrocardiogram sensor. Emerging sensors and data processing techniques appear promising for not only physical disease diagnosis but also psychiatric disorder screening in future medicine.

The objective of this special issue is to publish high-quality papers and promote researches in sensors and data processing techniques. Potential topics include but are not limited to the following: psychiatric disorder screening using sensors, sensors for daily stress monitoring, sensor-based data processing and diagnosis technique for future medicine and psychiatry, sensors designed for future medicine and psychiatry, application of conventional sensors for future medicine, sensor-based elderly monitoring in future super aging society, sensor application to robots used for elderly care at nursing care facilities and home, application of a microwave sensor for future medicine, sensor-based infection screening, emerging applications of infrared sensors in medical fields, and monitoring sensors for companion animals.

We welcomed papers not only biomedical sensing techniques but also diagnosing and therapeutic techniques based on sensor-determined vital signs.

The papers have been peer reviewed and have been selected on the basis of their quality and relevance to the topic of this special issue.

The paper "The Development of a Dual-Radar System with Automatic Hypopnea Threshold Optimization for Contact-Free Sleep Apnea-Hypopnea Syndrome Screening" deals with not only sleep apnea sensing techniques using dual radars located beneath bed mattress but also ideal screening algorism which determines the hypopnea threshold.

The clinical application of the developed portable vital sign monitoring system was achieved in the "Vital-SCOPE: Design and Evaluation of a Smart Vital Sign Monitor for Simultaneous Measurement of Pulse Rate, Respiratory Rate, and Body Temperature for Patient Monitoring."

The therapeutic aspects of sensor application for cancer therapy was achieved in "Thermal Sensor Circuit Using Thermography for Temperature-Controlled Laser Hyperthermia."

Monitoring techniques for domestic animals appeared in "Detection of Stress Hormone in the Milk for Animal Welfare Using QCM Method."

A paper which may not appear in the regular issue of this journal is also published in this special issue, the paper which utilized a game as a sensing tool for oral-facial malfunction, i.e., "An Innovative Serious Game for the Detection and Rehabilitation of Oral-Facial Malfunction in Children: A Pilot Study."

We hope that this special issue will be useful for researchers from the academia and the industry, standard developers, policy makers, professionals, and practitioners.

Conflicts of Interest

As the guest editorial team, we declare that there are no conflicts of interest or private agreements with companies regarding our work for this special issue. We have no financial relationships through employment and consultancies, either stock ownership or honoraria, with industry.

Takemi Matsui
Satoshi Suzuki
Guanghao Sun
Eddie Ng Yin Kwee

Hindawi
Journal of Sensors
Volume 2018, Article ID 4371872, 7 pages
https://doi.org/10.1155/2018/4371872

Research Article

Vital-SCOPE: Design and Evaluation of a Smart Vital Sign Monitor for Simultaneous Measurement of Pulse Rate, Respiratory Rate, and Body Temperature for Patient Monitoring

Guanghao Sun,[1] **Takemi Matsui**,[2] **Yasuyuki Watai**,[2] **Seokjin Kim**,[2] **Tetsuo Kirimoto**,[1] **Satoshi Suzuki**,[3] **and Yukiya Hakozaki**[4]

[1]*Graduate School of Informatics and Engineering, The University of Electro-Communications, Tokyo, Japan*
[2]*Graduate School of System Design, Tokyo Metropolitan University, Tokyo, Japan*
[3]*Department of Mechanical Engineering, Kansai University, Osaka, Japan*
[4]*Genkikai Yokohama Hospital, Yokohama, Japan*

Correspondence should be addressed to Guanghao Sun; guanghao.sun@uec.ac.jp

Received 5 August 2017; Revised 26 November 2017; Accepted 6 December 2017; Published 1 February 2018

Academic Editor: Armando Ricciardi

Consistent vital sign monitoring is critically important for early detection of clinical deterioration of patients in hospital settings. Mostly, nurses routinely measure and document the primary vital signs of all patients 2-3 times daily to assess their condition. To reduce nurse workload and thereby improve quality of patient care, a smart vital sign monitor named "Vital-SCOPE" for simultaneous measurement of vital signs was developed. Vital-SCOPE consists of multiple sensors, including a reflective photo sensor, thermopile, and medical radar, to be used in simultaneous pulse rate, respiratory rate, and body temperature monitoring within 10 s. It was tested in laboratory and hospital settings. Bland-Altman and Pearson's correlation analyses were used to compare the Vital-SCOPE results to those of reference measurements. The mean difference of the respiratory rate between respiratory effort belt and Vital-SCOPE was 0.47 breaths per minute with the 95% limit of agreement ranging from −7.4 to 6.5 breaths per minute. The Pearson's correlation coefficient was 0.63 ($P < 0.05$). Moreover, the mean difference of the pulse rate between electrocardiogram and Vital-SCOPE was 3.4 beats per minute with the 95% limit of agreement ranging from −13 to 5.8 beats per minute; the Pearson's correlation coefficient was 0.91 ($P < 0.01$), indicating strong linear relationship.

1. Introduction

Consistent vital sign monitoring is critically important for early detection of clinical deterioration in hospital settings [1]. In most hospitals, nurses routinely measure and document primary vital signs (e.g., pulse rate, oxygen saturation, respiratory rate, and body temperature) for all patients 2-3 times per day to make an assessment of the patient's condition [2, 3]. However, such measurement and documentation is a repetitive and time-consuming task for nurses [4]. They use different medical devices such as an electronic thermometer to measure body temperature and a pulse oximeter to measure heart rate and oxygen saturation. In particular, the measurement of respiratory rate is often omitted because having nurses count the chest wall movement in a busy hospital setting is not efficient [5, 6]. To reduce the workload of the nurses and thus improve the quality of patient care, we developed a smart vital sign monitor for simultaneous measurement of pulse rate, respiratory rate, and body temperature.

In our previous studies, we proposed a multiple vital sign-based infection screening system with sensor fusion technology that can rapidly perform medical inspections at places of mass gatherings, such as airport quarantine stations

and outpatient units [7–10]. This multiple sensor system consists of a medical radar and an infrared thermographic camera. Pulse and respiratory rates were measured using a 24 GHz medical radar, and body surface temperature was monitored using a thermographic camera without contacting the patient. We tested the system on patients with seasonal influenza in case-controlled studies and showed that the detection sensitivity ranged from 81.5% to 98.0%. The advantages of this system include the following: (1) rapid and simultaneous measurement of multiple vital signs within 10 s; (2) a noncontact measurement scheme for reducing the physical and mental burden of patients considerably; and (3) automatic detection of clinical deterioration with optimal discriminant analysis.

These advantages compelled us to redesign the infection screening system to create a smart, portable, and easy-to-use vital sign monitor for patient monitoring. To miniaturize the vital sign monitor, an onboard field programmable gate array (FPGA) microcontroller was used to acquire and process the biosignals from multiple sensors. In addition, we integrated multiple sensors (reflective photo sensor, thermopile, and 24 GHz medical radar) and a FPGA microcontroller into a small disc-shaped form similar to a stethoscope, thus arriving at the name "Vital-SCOPE." Throughout the remainder of this paper, we describe the design concept of Vital-SCOPE and report the validation of this system in both laboratory and hospital settings.

2. Material and Methods

2.1. The Design Concept and Hardware Configuration of Vital-SCOPE. Vital-SCOPE simultaneously measures pulse rate, respiratory rate, and body temperature when the sensor unit is placed on the carotid artery area of the neck and provides results within 10 s (Figure 1). The Vital-SCOPE sensor unit consists of a 24 GHz medical radar (SHARP, DC6M4JN3000, Japan), reflective photo sensor (Pulse Sensor, SEN-11574, SparkFun), and thermopile contactless temperature sensor (NIPPON CERAMIC, TSUP-A1D01S-50-60, Japan). The respiratory rate is measured with a 24 GHz medical radar by monitoring the chest surface movements. Note that the output power of the 24 GHz medical radar is 10 mW with an electric power density of 1.5×10^{-2} mW/cm^2 at the carotid artery area of the neck, which is much lower than the Japanese safety guideline for radio-radiation protection. The reflective photo sensor is used to measure pulse rate from the carotid artery, and the body surface temperature is measured using the thermopile. The disc-shaped sensor unit is 5.5 cm in diameter and 6.0 cm in height and can be easily used in one-handed operations.

A block diagram of Vital-SCOPE is illustrated in Figure 2. A myRIO-embedded device from National Instruments [11] is used to control the entire system; myRIO includes analog inputs, a WiFi module, Xilinx FPGA, and a dual-core ARM Cortex-A9 processor. As shown in Figure 2, the body temperature value is the output from the thermopile and is sent to myRIO via I2C communications. Simultaneously, the respiratory and pulse signals measured by the 24 GHz medical radar and photo sensor are converted to digital signals with a sampling rate of 100 Hz for data transfer via the IO ports. Moreover, a signal-processing printed circuit board (PCB) was designed to amplify the 24 GHz medical radar signal, as well as a band-pass filter to eliminate DC components and high-frequency noise (set between 0.1 Hz and 0.7 Hz for respiration signal). The raw data acquired by the multiple sensors were saved in an external USB flash drive connected to myRIO inside the device. The calculated pulse rate, respiratory rate, and body temperature are sent wirelessly using the WiFi module to a tablet PC in real time, where automated documentations of the vital signs are stored and displayed. The battery consumption is important for designing such a hand-held system. The multiple sensors and the myRIO-embedded device have low current consumption of between 1000 and 1500 mA. In this work, an 8400 mAh mobile battery was used for powering the system, which means that the system lasts for approximately 5.6 hours in continuous use. The myRIO-embedded device and battery are placed in the controller unit. The controller unit is 25.0 cm in width, 10.5 cm in depth, and 24.0 cm in height.

2.2. Evaluation of Vital-SCOPE in Laboratory and Hospital Settings. The evaluation of Vital-SCOPE was conducted in both laboratory and hospital settings. Ten graduate students (22.7 ± 1.3 years of age) participated in the laboratory test at Tokyo Metropolitan University. To cover a wide range of pulse and respiratory rates, the test procedure was divided into two sessions. First, the subjects were tested at rest, and second, the subjects were tested just after exercising. The exercise trial consisted of the subjects using a bicycle ergometer at 100 W for 15 min after taking the measurement during a resting state, thereby elevating the pulse and respiratory rates. Their respiratory rate, pulse rate, and body surface temperature were measured by Vital-SCOPE; reference measurements were simultaneously obtained using a contact-type electrocardiogram (ECG) (GMS, LRR-03, Japan) and a respiratory effort belt (NIHON KOHDEN, TR-512, Japan). In order to evaluate the viability of Vital-SCOPE in a hospital setting, we tested it with 11 inpatients (72.2 ± 15.5 years of age) at Yokohama Hospital in February 2017 for one week. The Yokohama Hospital is a recuperation hospital for care of older people. This study was approved by the Ethics Committee of the Yokohama Hospital and the Committee on Human Research of the Faculty of System Design, Tokyo Metropolitan University. All subjects gave their informed written consent.

2.3. Statistical Analysis. The Bland-Altman and Pearson's correlation analysis were used to compare Vital-SCOPE to the reference measurements obtained using the MATLAB Statistics and Machine Learning Toolbox (MathWorks, Natick, MA, USA). The Bland-Altman analysis is a simple and efficient method to assess the agreement between two measurements in clinical studies [12]. A P value of less than 0.05 is considered to indicate statistical significance.

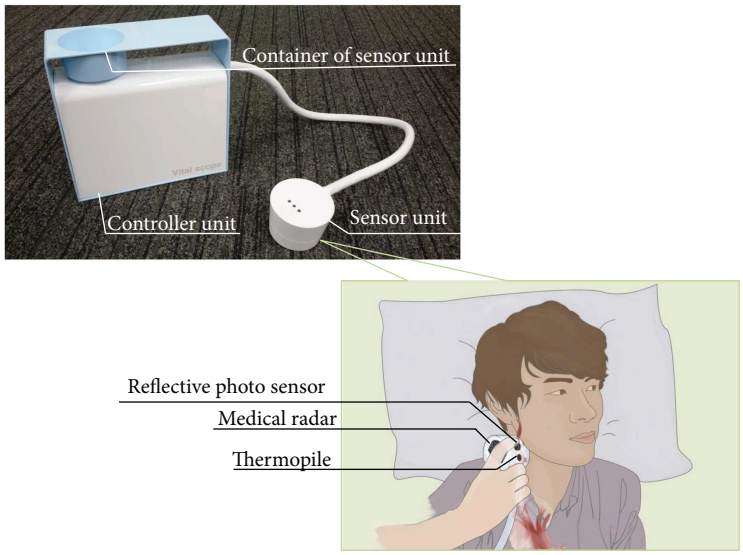

Figure 1: Design concept and hardware configuration of Vital-SCOPE.

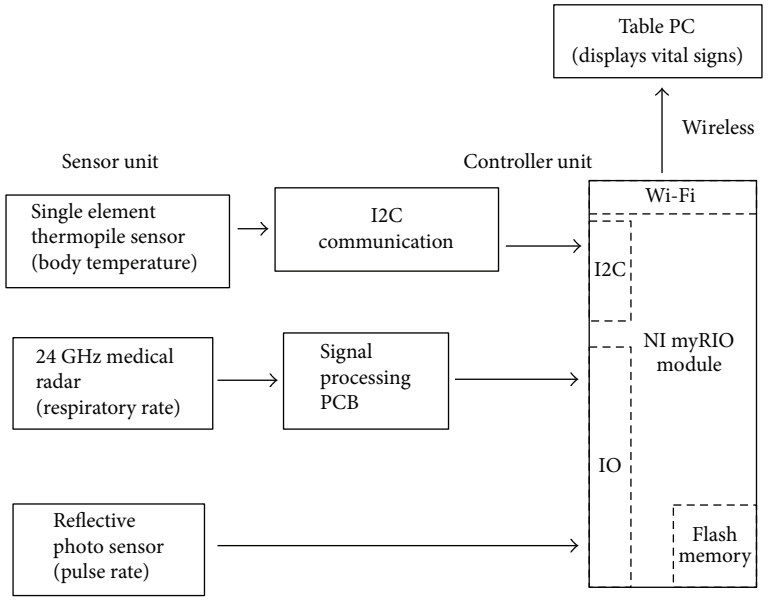

Figure 2: Block diagram of Vital-SCOPE.

3. Results

Figure 3 shows the Bland-Altman and Pearson's correlation plots for ten participants with 160 pairs of respiratory rate (resting condition only) and 320 pairs of pulse rate (rest and after exercising) measurements in the laboratory. The mean difference of the respiratory rate between the respiratory effort belt and Vital-SCOPE was 0.47 breaths per minute (bpm) with the 95% limit of agreement ranging from −7.4 to 6.5 bpm. The Pearson's correlation coefficient was 0.63 ($P < 0.05$), indicating a moderately strong linear relationship. Moreover, the mean difference of the pulse rate between the ECG and Vital-SCOPE was 3.4 beats per minute (bpm) with the 95% limit of agreement ranging from −13 to 5.8 bpm; the Pearson's correlation coefficient was 0.91 ($P < 0.01$) showing a strong linear relationship. Figure 4 shows a comparison of the pulse and respiratory signals measured using Vital-SCOPE, ECG, and the respiratory effort belt. The peaks of the signal pulse were similar to the R-R interval in an ECG signal. In addition, the respiratory signal measured using a medical radar within 10 s indicated a high correlation with the signal measured by the respiratory effort belt.

We also evaluated the usability of Vital-SCOPE in a hospital setting where the nurses checked the vital signs of patients every day for a week. Table 1 presents the historical trends of pulse rate, respiratory rate, and body surface

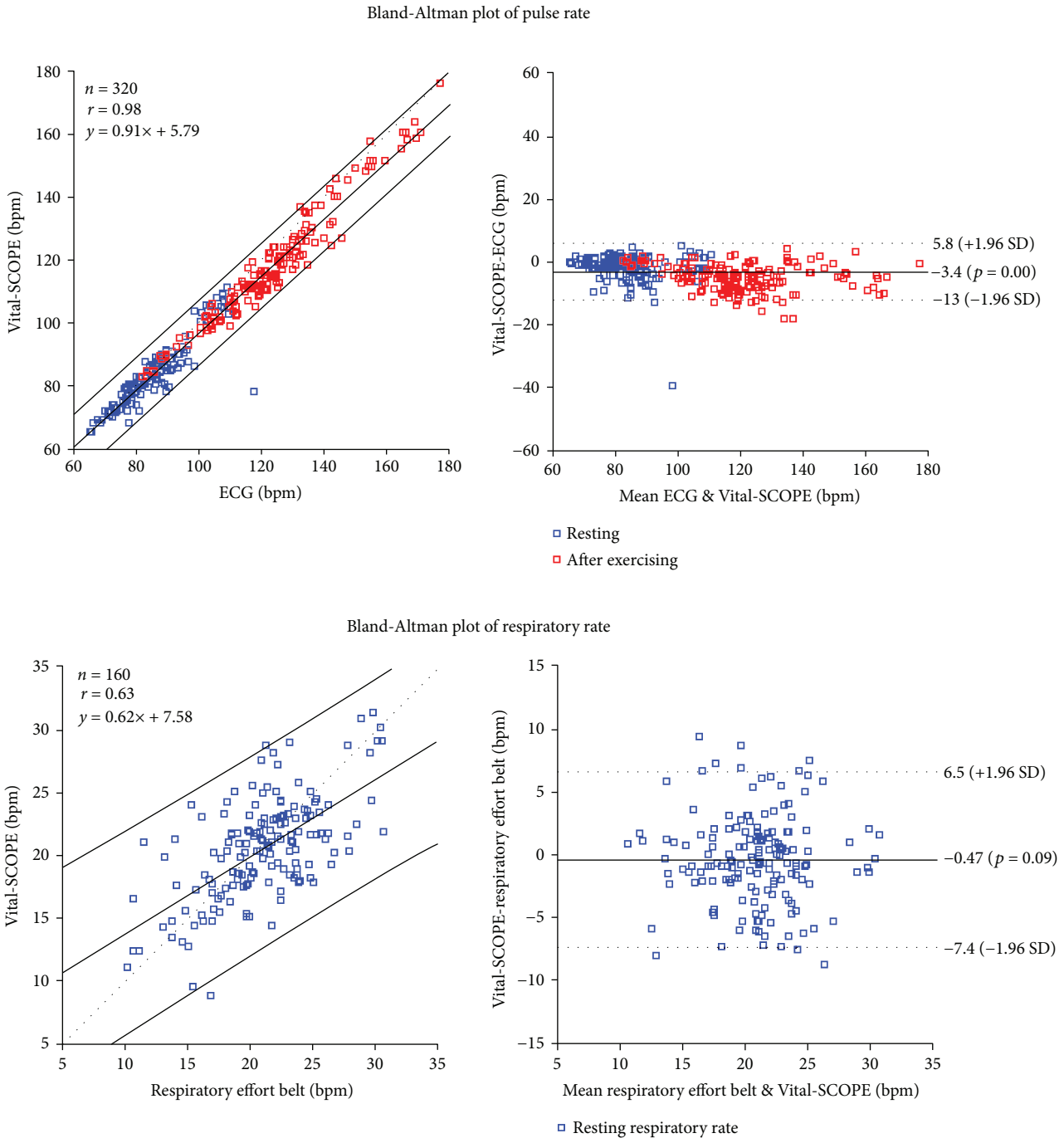

Figure 3: Bland-Altman and Pearson's correlation plots of Vital-SCOPE, ECG, and respiratory effort belt.

temperature measured via Vital-SCOPE for four patients at Yokohama Hospital. The comparison of the body surface temperature and axillary temperature showed an average mean difference of 1.5°C, owing to the body surface temperature being lower than the core temperature [13]. As observed in Table 1, patient B had a fever (axillary temperature: 38.5°C, body surface temperature: 37.1°C) on February 24, 2017, indicating that Vital-SCOPE accurately captured the elevated body temperature.

4. Discussion

In this paper, a vital sign monitor was proposed for patient monitoring that simultaneously measures pulse rate, respiratory rate, and body temperature. We investigated the use of Vital-SCOPE in laboratory and hospital settings and compared the vital sign measurements with reference devices. The results showed that Vital-SCOPE provides the possibility of accurate vital sign measurements that can reduce the

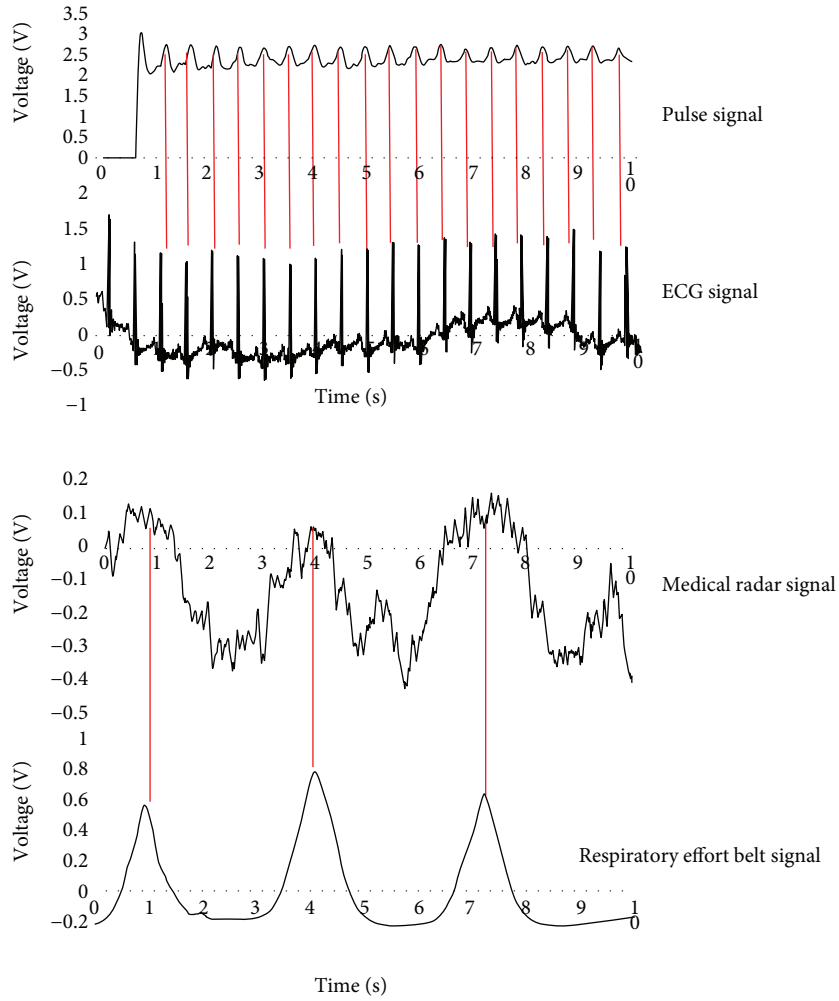

Figure 4: A comparison of the pulse and respiratory signals measured via Vital-SCOPE, ECG, and respiratory effort belt.

workload of nurses and improve patient care. Contact-type ECG and respiratory belt transducer have become universally accepted standard for measuring heart and respiratory rates. However, such measurements require the attachment of sensors, which can cause discomfort and place a heavy burden on patient. In recent years, a variety of unobtrusive medical sensors have been developed for long-term or intermittent physiological measurements, including RGB visible and thermal images for measuring heart and respiratory rates [7] and measurement of cardiac and respiration pulses using laser Doppler or a microwave medical radar [14, 15]. These noncontact sensors have their advantages and disadvantages depending on the specific applications. In this study, we adopted a medical radar combined with a reflective photo sensor and thermopile to measure multiple vital signs; this sensor fusion device offered advantages of vital sign information integration for early detection of clinical deterioration in hospital settings.

To date, body temperature, pulse rate, and oxygen saturation are usually checked by nurses using an electronic thermometer and pulse oximeter. However, the measurement of the respiratory rate is often omitted because it is not efficient in busy hospital settings. Recent studies indicated that a respiratory rate higher than 27 bpm is an important predictor of cardiac arrest for inpatients in hospital settings [16]. To meet this need, we designed Vital-SCOPE not only to measure body temperature and pulse rate but also for noncontact measurement of the respiratory rate using a medical radar. Because a medical radar is a noncontact-type sensor, the measurement significantly reduced the physical and psychological burden on patients. In this study, as shown in Table 1, the pulse rate and body temperature of some patients were near normal. However, their respiratory rate was higher than 27 bpm with irregular respiratory rhythms. In a case like this, Vital-SCOPE, which simultaneously monitors multiple vital signs including respiratory rate, may offer an early identification of patients who are at risk of clinical deterioration. In addition, Vital-SCOPE combines vital sign acquisition and automatic documentation, helping nurses make their work more efficient.

In this study, we showed the design concept and basic architecture of Vital-SCOPE, but there are several potential limitations of our current system. (1) In such embedded system, to reduce the usage of energy, the minimum sampling rate (in this study 100 Hz) is required but without

Table 1: The historical trends of vital signs measured via Vital-SCOPE for four patients at a hospital setting.

	Day	Age	Gender	Respiration rate (bpm)	Pulse rate (bpm)	Body surface temperature (°C)	Axillary temperature (°C)
Patient A	2017/2/21	81	Male	27	77	32.0	37.8
	2017/2/22	81	Male	27	73	34.4	35.2
	2017/2/23	81	Male	22	67	34.6	35.9
	2017/2/24	81	Male	16	74	34.2	35
	2017/2/25	81	Male	20	95	34.7	36.6
Patient B	2017/2/21	85	Male	27	78	35.4	37.1
	2017/2/22	85	Male	23	90	35.3	36.6
	2017/2/23	85	Male	27	62	35.0	36.9
	2017/2/24	85	Male	28	71	37.1	38.5
	2017/2/25	85	Male	23	63	35.3	35.4
Patient C	2017/2/21	92	Female	22	83	36.8	37.3
	2017/2/22	92	Female	26	87	35.4	37.9
	2017/2/23	92	Female	25	67	36.1	37.2
	2017/2/24	92	Female	21	75	36.7	36.6
	2017/2/25	92	Female	28	79	35.5	37.4
Patient D	2017/2/21	68	Female	25	75	34.7	35.6
	2017/2/22	68	Female	13	84	34.4	36.2
	2017/2/23	68	Female	23	91	34.6	35.8
	2017/2/24	68	Female	34	75	33.8	35.1
	2017/2/25	68	Female	32	76	35.5	36

compromising the accuracy. (2) Regarding the automatic documentation of measured vital signs, we adopted the Data Dashboard for LabVIEW app on a tablet PC to visualize the data; but we are still working on designing an easy-to-use graphical user interface for nurses. (3) In this study, we focused on evaluating the measurement accuracy of the system, however without including the function of automatic detection of clinical deterioration. In our near future work, we will include the national early warning score (NEWS) to our system based on measured vital signs. The NEWS score was introduced by the Royal College of Physicians in London; the score parameters include respiratory rate, oxygen saturation level, body temperature, blood pressure, and heart rate. The higher score indicates higher risk and significant clinical deterioration [17]. To this time, our system only measures three parameters of NEWS score; we will add other vital signs such as blood pressure and oxygen saturation in our next work.

5. Conclusion

In summary, a multiple vital sign monitor "Vital-SCOPE" was designed for patient monitoring. Because the system simultaneously monitors pulse rate, respiratory rate, and body temperature within 10 s and automatically documents the vital signs, it has high potential for use as an important tool in patient monitoring in a hospital setting.

Conflicts of Interest

The authors have no conflict of interest.

Acknowledgments

This study was supported by a Grant-in-Aid for Young Scientists (16K16363) funded by the Ministry of Education, Culture, Sports, Science and Technology of Japan. The authors are grateful to the nursing staff at Yokohama Hospital for their contribution to this study.

References

[1] M. Elliott and A. Coventry, "Critical care: the eight vital signs of patient monitoring," *British Journal of Nursing*, vol. 21, no. 10, pp. 621–625, 2012.

[2] W. Q. Mok, W. Wang, and S. Y. Liaw, "Vital signs monitoring to detect patient deterioration: an integrative literature review," *International Journal of Nursing Practice*, vol. 21, no. S2, pp. 91–98, 2015.

[3] T. Watkins, L. Whisman, and P. Booker, "Nursing assessment of continuous vital sign surveillance to improve patient safety on the medical/surgical unit," *Journal of Clinical Nursing*, vol. 25, no. 1-2, pp. 278–281, 2016.

[4] L. Rose and S. P. Clarke, "Vital signs," *The American Journal of Nursing*, vol. 110, no. 5, p. 11, 2010.

[5] S. Cooper, R. Cant, and L. Sparkes, "Respiratory rate records: the repeated rate?," *Journal of Clinical Nursing*, vol. 23, no. 9-10, pp. 1236–1238, 2014.

[6] M. A. Cretikos, R. Bellomo, K. Hillman, J. Chen, S. Finfer, and A. Flabouris, "Respiratory rate: the neglected vital sign," *The Medical Journal of Australia*, vol. 188, no. 11, pp. 657–659, 2008.

[7] G. Sun, Y. Nakayama, S. Dagdanpurev et al., "Remote sensing of multiple vital signs using a CMOS camera-equipped infrared thermography system and its clinical application in rapidly screening patients with suspected infectious diseases," *International Journal of Infectious Diseases*, vol. 55, pp. 113–117, 2017.

[8] G. Sun, T. Matsui, Y. Hakozaki, and S. Abe, "An infectious disease/fever screening radar system which stratifies higher-risk patients within ten seconds using a neural network and the fuzzy grouping method," *The Journal of Infection*, vol. 70, no. 3, pp. 230–236, 2015.

[9] Y. Yao, G. Sun, T. Matsui, Y. Hakozaki, S. van Waasen, and M. Schiek, "Multiple vital-sign-based infection screening outperforms thermography independent of the classification algorithm," *IEEE Transactions on Biomedical Engineering*, vol. 63, no. 5, pp. 1025–1033, 2016.

[10] T. Matsui, Y. Hakozaki, S. Suzuki et al., "A novel screening method for influenza patients using a newly developed non-contact screening system," *Journal of Infection*, vol. 60, no. 4, pp. 271–277, 2010.

[11] G. Sun, Y. Watai, and T. Matsui, "Development of a wireless physiological computing platform using National Instruments' myRIO embedded device," in *Proceedings of 2015 IEEE 4th Global Conference on Consumer Electronics*, pp. 27–30, Osaka, Japan, October 2015.

[12] D. Giavarina, "Understanding Bland Altman analysis," *Biochemia Medica*, vol. 25, no. 2, pp. 141–151, 2015.

[13] G. Sun, T. Matsui, T. Kirimoto, Y. Yao, and S. Abe, "Applications of infrared thermography for noncontact and noninvasive mass screening of Febrile International Travelers at airport quarantine stations," in *Application of Infrared to Biomedical Sciences*, Y. K. Ng and M. Etehadtavakol, Eds., pp. 347–358, Springer, Singapore, 2017.

[14] C. Li, V. M. Lubecke, O. Boric-Lubecke, and J. Lin, "A review on recent advances in Doppler radar sensors for noncontact healthcare monitoring," *IEEE Transactions on Microwave Theory and Techniques*, vol. 61, no. 5, pp. 2046–2060, 2013.

[15] S. Ulyanov and V. Tuchin, "Pulse-wave monitoring by means of focused laser beams scattered by skin surface and membranes," in *Proceedings SPIE 1884, Static and Dynamic Light Scattering in Medicine and Biology*, pp. 160–168, Los Angeles, CA, 1993.

[16] J. F. Fieselmann, M. S. Hendryx, C. M. Helms, and D. S. Wakefield, "Respiratory rate predicts cardiopulmonary arrest for internal medicine inpatients," *Journal of General Internal Medicine*, vol. 8, no. 7, pp. 354–360, 1993.

[17] S. Uppanisakorn, R. Bhurayanontachai, J. Boonyarat, and J. Kaewpradit, "National Early Warning Score (NEWS) at ICU discharge can predict early clinical deterioration after ICU transfer," *Journal of Critical Care*, vol. 43, pp. 225–229, 2017.

Hindawi
Journal of Sensors
Volume 2018, Article ID 8210502, 8 pages
https://doi.org/10.1155/2018/8210502

Research Article

The Development of a Dual-Radar System with Automatic Hypopnea Threshold Optimization for Contact-Free Sleep Apnea-Hypopnea Syndrome Screening

Shinji Gotoh,[1] **Takemi Matsui**,[2] **Yoshikazu Naka**,[3] **and Osamu Kurita**[3]

[1]*Department of Planning and Development, TAU GIKEN Co. Ltd., 814 Saedo-cho, Tsuzuki-ku, Yokohama, Kanagawa 224-0054, Japan*
[2]*Faculty of System Design, Tokyo Metropolitan University, 6-6 Asahigaoka, Hino, Tokyo 191-0065, Japan*
[3]*Tomei Atsugi Hospital, 243-8571 232 Funako, Atsugi, Kanagawa, Japan*

Correspondence should be addressed to Shinji Gotoh; s-gotoh@taugiken.jp

Received 29 August 2017; Accepted 10 December 2017; Published 8 January 2018

Academic Editor: Romeo Bernini

Full-night polysomnography (PSG) examination is regarded as the gold standard for the diagnosis of sleep apnea-hypopnea syndrome (SAHS). However, PSG requires the placement of multiple sensors on the head, face, and chest, which can impose a heavy strain on patients. Therefore, in the present study, we aimed to develop a contact-free, stand-alone SAHS screening system that eliminates body movement artifacts based on automatic optimization of the hypopnea threshold. Doppler radar sensors were placed beneath a mattress. In order to achieve high sensitivity and specificity, the hypopnea was based on the average amplitude of respiration during the full sleep period. The threshold was determined via receiver operating characteristic (ROC) analysis using PSG as a reference. We conducted full-night clinical tests of the proposed system in 27 patients with suspected SAHS (49 ± 12 years) at Tomei Atsugi Hospital. When predicting the severity of SAHS with an apnea-hypopnea index (AHI) of >30/h using PSG as a reference, the proposed system achieved a sensitivity of 100% and a specificity of 100%. These results represent a drastic improvement over those of our previous study (sensitivity: 90%; specificity: 79%).

1. Introduction

Sleep disorders such as sleep apnea-hypopnea syndrome (SAHS) were first recognized as an important public health concern in the late 1970s [1]. Since its approval for clinical use, polysomnography (PSG) examination has been regarded as the gold standard for the diagnosis of SAHS. However, PSG requires the placement of multiple sensors on the head, face, and chest, which can impose a heavy strain on patients. To address these issues, early research focused on the development of clinically useful microwave radar (radar) systems for monitoring vital signs and body movements during sleep [2, 3]. Although research regarding contact-free, radar-based respirometry and heart rate monitoring proved promising in the early 2000s, most studies at this time were laboratory investigations [4–6], and clinical studies did not begin until the first decade of the twenty-first century [7, 8]. However, in the late 1990s, our research group began to investigate the use of Doppler radar-based respirometry for identifying survivors trapped beneath debris following massive earthquakes. Our findings indicated that this system, which utilizes antennae that can be inserted into heavy debris, exhibited high sensitivity for the identification of survivors [9, 10].

Based on these findings, we began to investigate the applicability of small microwave Doppler radar modules for the measurement of human vital signs [7, 11, 12]. In our recent studies, we compared the clinical usefulness of radar and CO_2 sensors [13], radar and SpO_2 sensors [14], and radar and PSG [15]. As the absolute values of respiration amplitude change depending on sleep state or changes in posture, we developed a method for detecting hypopnea based on *relative decreases* in amplitude every 30 seconds, without the use of a baseline value. Although this method yielded relatively good

results [14], artifacts associated with body movement remained, resulting in low specificity. Several other research groups have also attempted to eliminate interference caused by body movement during sleep [16–18], with limited success. Also, Anishchenko et al. [19] proposed artifact removal method using Toeplitz matrix for rodents' respiratory activity in laboratory. Baboli et al. [20] presented radar monitoring system integrated with PSG system. Zhang et al. [21] proposed sleep stages classification using deep learning with bagged tree algorithm applied to laboratory experiments; participants were a couple of subjects. Beattie et al. [22] presented successful accurate scoring of AHI using load cells under the supports of bed. They achieved 100% sensitivity and 97% specificity, at cutoff PSG AHI > 30. However, their classification was conducted by subjective assessment.

Although the use of additional biometric data may allow for the comprehensive elimination of noise based on the timing of body movements [16–18], no single system to date has achieved this aim. Therefore, in the present study, we aimed to develop a stand-alone screening system for the elimination of body movement artifacts based on automatic optimization of the hypopnea threshold. In this system, candidate events (i.e., relative decreases in amplitude) are filtered out based on an individual threshold derived from full sleep-span data.

2. Materials and Methods

2.1. Configuration of the System. To overcome the effects of posture change during sleep, we utilized two radar systems to ensure that respiration was always detected by at least one sensor (MVM, TAU GIKEN Co. Ltd. Yokohama, Japan; Doppler module NJR 4169J, New Japan Radio Co. Ltd., Tokyo, Japan). The system configuration is depicted in Figure 1(a). The system specifications were as follows: (a) emitting frequency of 10.525 GHz, (b) emitting power of approximately 10 mW, and (c) antenna gain of 5 dBi. Using quadrature direct conversion technique [23, 24], received signals were converted into in-phase output and quadrature output. Then, these outputs were filtered by analog band-pass filters, where adjusting processes to balance amplitude of both output and to eliminate phase noise were also conducted. The two radar sensors were located beneath the mattress, 20 cm from the left and right of the midline of the participant's body, near the iliac bone (Figure 1(b)). Data from the two radar systems were integrated following measurement.

The 10.525 GHz radar output was filtered and digitized in the main unit at a rate of 20 times/s. The data were transferred to a personal computer via wireless LAN and stored as CSV files (Figure 1(c)). Following data collection, offline calculations were performed in Microsoft Excel to identify signs of respiratory disorders. The stored files consisted of the formatted data with time stamps every 0.05 s. The total number of data points was approximately 576,000 (i.e., 20 times $s^{-1} \times 60\,s \times 60\,m \times 8\,h$).

2.2. Automatic Optimization of Hypopnea Threshold. In order to achieve high sensitivity and specificity for the detection of SAHS, we developed a novel tool for automatic optimization of the hypopnea threshold. Data were analyzed using Microsoft Excel, in accordance with the following protocol: The quadrature detector output values E_I and E_Q (E_I = in-phase output, E_Q = quadrature output) were used to calculate the phase deviation of the received signal. E_I and E_Q values were obtained for each stored data point. Using E_I and E_Q, the phase of respiration was calculated according to (1), where $\theta(t)$ (degrees) represents the phase at time t (s) and atan represents the arctangent in radians:

$$\theta(t) = \operatorname{atan}\left(\frac{E_Q}{E_I}\right) \cdot \frac{180}{\pi}. \tag{1}$$

Amplifiers and filters were driven by a single 5 V DC power source. A center value of 2.5 V was used for output signals, resulting in periodic vibration of $\theta(t)$ at a center value of 45 degrees. Then, the magnitude of respiration over 5 s ($m(t)$ in degrees) was calculated according to (2), where $\Delta t = 0.05$ s:

$$\begin{aligned} m(t) = \{&\max[\theta(t), \theta(t+\Delta t), \ldots, \theta(t+5)] \\ &- \min[\theta(t), \theta(t+\Delta t), \ldots, \theta(t+5)]\}. \end{aligned} \tag{2}$$

The functions max[ ] and min[ ] were used to extract the maximum and minimum values, respectively.

Using three $m(t)$ values, $M(t)$ and $M(t-15)$ were calculated in degrees as follows:

$$\begin{aligned} M(t) &= \frac{m(t) + m(t+5) + m(t+10)}{3}, \\ M(t-5) &= \frac{m(t-15) + m(t-10) + m(t-5)}{3}. \end{aligned} \tag{3}$$

Then, the event markers $E(t)$ were calculated as follows:

$$\begin{aligned} &\text{IF } \frac{M(t-15)}{M(t)} \geq 2 \text{ AND } \{\max[m(t), m(t+5), m(t+10), m \\ &\cdot(t-5), m(t-10), m(t-15)] < \mu\}, \\ &\qquad E(t) = 1, \text{else } E(t) = 0, \end{aligned} \tag{4}$$

where μ was calculated as

$$\mu = K \cdot \frac{1}{L} \cdot \sum_{n=0}^{L-1} m(0 + n \cdot \Delta t). \tag{5}$$

As shown in (5), μ represented average amplitude of overall sleeping time.

K was determined to optimize sensitivity and specificity via receiver operating characteristic (ROC) analysis based on SAHS patients' data using PSG as a reference. L represented the approximate number of data points (576,000), and $\Delta t = 0.05$ s. The $E(t)$ was calculated every 30 seconds and stored in the data file, and the consecutive portions of $E(t) = 1$ were counted as a single event. Separate $E(t)$ values were calculated for radar1 and radar2 ($E(t)_{\text{radar1}}$ and $E(t)_{\text{radar2}}$, resp.). To integrate the data from the two radar

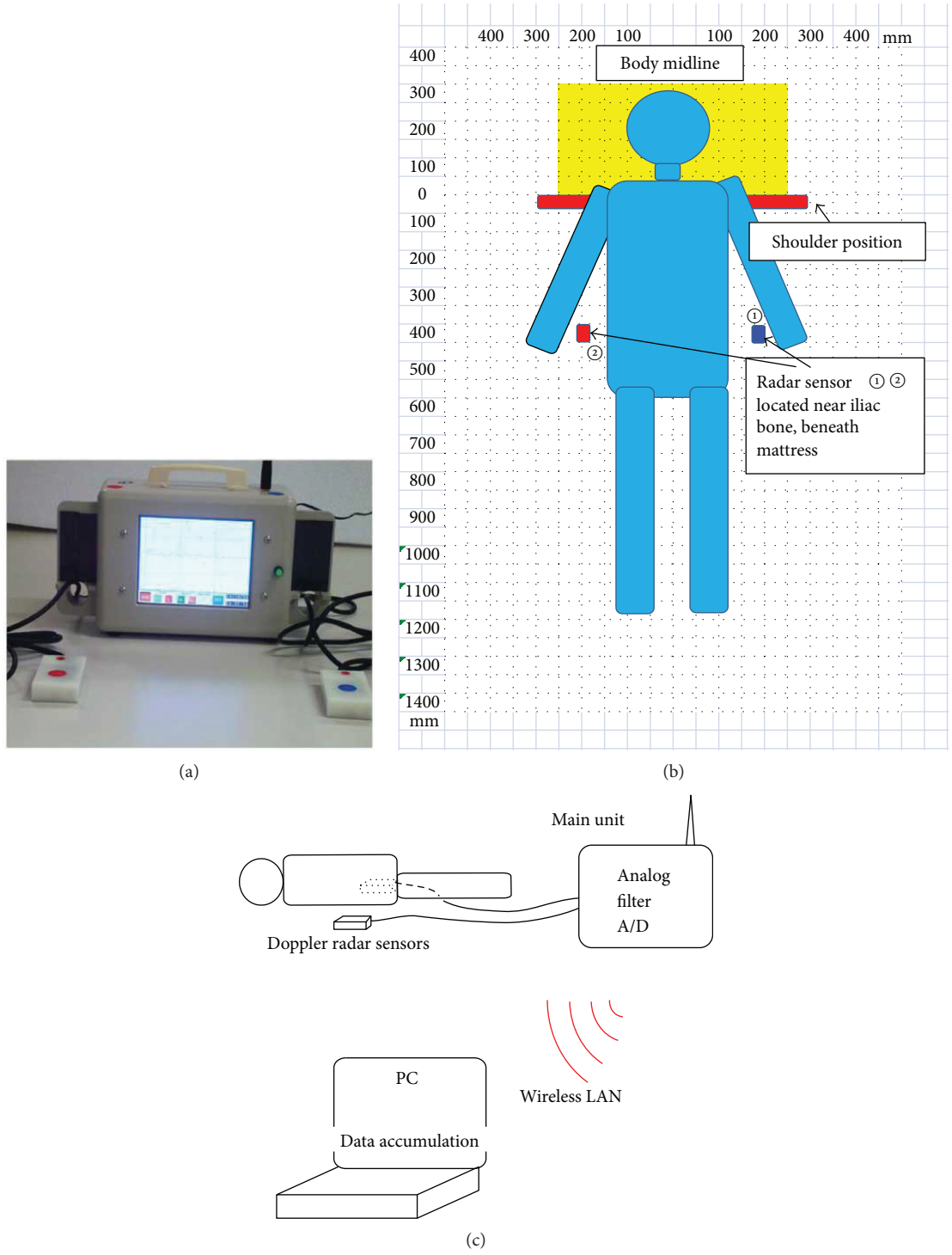

FIGURE 1: The dual Doppler radar system. (a) A picture of the main unit and sensors. (b) The sensors were located 20 cm to the left and right of the patient's midline, near the iliac bone. (c) Schematic of respiration measurement.

systems, the logical sum of these values was then calculated in Excel as follows:

$$E(t)_{\text{merged}} = E(t)_{\text{radar1}} \cup E(t)_{\text{radar2}}. \quad (6)$$

Finally, $E(t)_{\text{merged}}$ values of 1 were considered indicative of respiratory disorder.

A value of $(M(t-15)/M(t)) \geq 2$ was considered indicative of hypopnea based on the $\text{AHI}_{\text{Chicago}}$ criteria provided by the American Academy of Sleep Medicine (AASM), in which hypopnea is indicated by >50% reduction in air flow for more than 10 s, >3% oxygen desaturation, or arousal. Although radar measurements of body surface area are associated with airflow, they do not exhibit one-to-one

Table 1: Number of radar detected hypopnea events.

Participant	AHI by PSG	Average amplitude (degree)		Number of radar detected events corresponding to K value							Before optimizing
		Radar1	Radar2	$K = 0.25$	$K = 0.5$	$K = 0.75$	$K = 1.0$	$K = 1.25$	$K = 1.5$	$K = 1.75$	
1	8.3	5.8	4.8	4	17	48	65	75	92	108	161
2	12.0	7.9	7.1	25	46	62	74	76	80	83	102
3	14.0	6.3	5.6	22	56	80	100	120	137	155	246
4	15.6	4.5	4.9	10	43	65	85	106	121	129	144
5	15.6	4.2	2.5	24	62	99	122	138	156	167	211
6	19.2	3.3	5.3	16	49	82	107	124	145	149	174
7	20.0	8.2	5.9	23	62	90	118	131	163	172	191
8	20.2	2.9	2.4	6	29	71	112	141	152	161	173
9	21.8	4.8	4.8	26	69	95	111	136	163	189	259
10	26.0	4.8	2.7	21	57	79	90	104	118	122	160
11	26.0	3.3	3.8	7	60	105	159	198	240	260	358
12	28.5	4.7	3.8	21	61	88	114	140	160	170	184
13	29.2	3.5	3.5	49	105	142	160	182	192	204	236
14	29.9	3.0	2.5	6	55	105	137	158	175	189	194
15	37.7	7.0	6.7	60	126	169	199	233	264	285	301
16	39.2	7.5	6.2	76	257	399	501	567	612	651	744
17	39.6	16.2	19.1	54	152	235	320	383	421	460	466
18	39.6	10.9	12.9	113	296	424	512	575	619	663	673
19	43.2	7.9	3.9	14	57	114	162	190	207	221	276
20	47.6	5.0	11.7	63	173	268	335	377	431	455	497
21	59.5	6.3	5.9	28	85	162	234	284	321	349	398
22	59.5	5.1	8.3	56	148	221	269	308	333	350	386
23	64.0	3.9	4.0	65	197	314	358	381	389	405	414
24	67.5	12.4	17.5	94	220	313	416	500	555	615	584
25	68.1	9.0	11.6	33	117	161	189	213	233	244	212
26	71.4	13.0	9.7	178	402	562	687	761	828	878	936
27	99.2	12.1	11.0	136	266	368	456	503	537	559	595

Column 2: individual apnea-hypopnea index obtained via PSG. Columns 3 and 4: the average radar-detected respiration amplitude. Columns 5 to 11: number of radar-detected events corresponding to K value. Column 12: radar detected events before automatic normal-hypopnea threshold optimization.

correspondence with airflow due to changes in the distance/angle between the radar sensors and the body. Thus, we were unable to utilize the revised AASM 2012 criteria, which specify apnea and hypopnea threshold values of 90% and 30% decreases in amplitude relative to baseline, respectively. Although these criteria may be applicable when patients do not change posture or for measurement during a single stage of sleep, we considered these criteria too stringent for radar-based measurement. Therefore, simplified criteria were adopted to identify cases of probably sleep-disordered breathing in the present and previous studies [14, 15].

Thus, the optimizer first identified candidates for respiratory disorder, following which it evaluated these candidates based on K and μ.

2.3. Clinical Testing and K Value Optimization. We conducted clinical tests of the proposed system in 27 patients (mean age: 49 ± 12 years; 22 men, 5 women) hospitalized one night for the evaluation of suspected SAHS from May to September of 2014 and February to March of 2015. All patients provided written informed consent to participate in the present study. Patients underwent simultaneous evaluation via PSG (Sleep Watcher E-series, Compumedics Ltd., Victoria, Australia; data processing: Teijin Pharma Ltd., Tokyo, Japan) and radar-based screening. The PSG determines AHIs based on AASM 2012 criteria [25]. The duration of measurement was 8 h in all cases. This study was approved by the Ethics Committee of Tomei Atsugi Hospital (Atsugi, Kanagawa, Japan).

Receiver operating characteristic (ROC) analysis was conducted to determine the appropriate K value. K values were increased from 0.25 to 1.75 in increments of 0.25, and the number of derived $E(t)_{\text{merged}}$ events was calculated at each step. The results of this process are summarized in Table 1. PSG-based diagnoses were used in conjunction with R version 3.3.3. and ROCR 1.0-5 library to select the conditions most appropriate for determining an AHI $\geq$ 30/h. A K

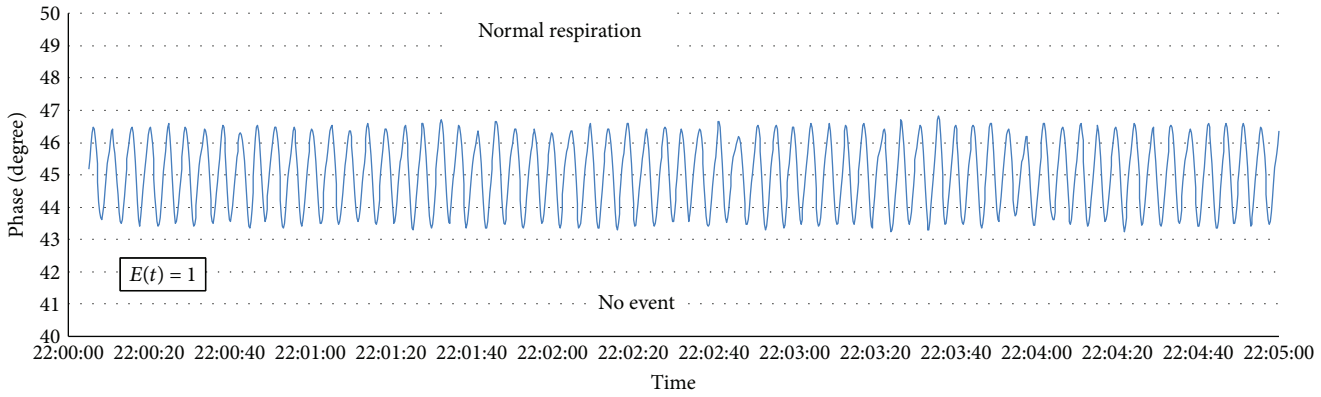

Figure 2: Typical sample of normal respiration. AHI = 14.

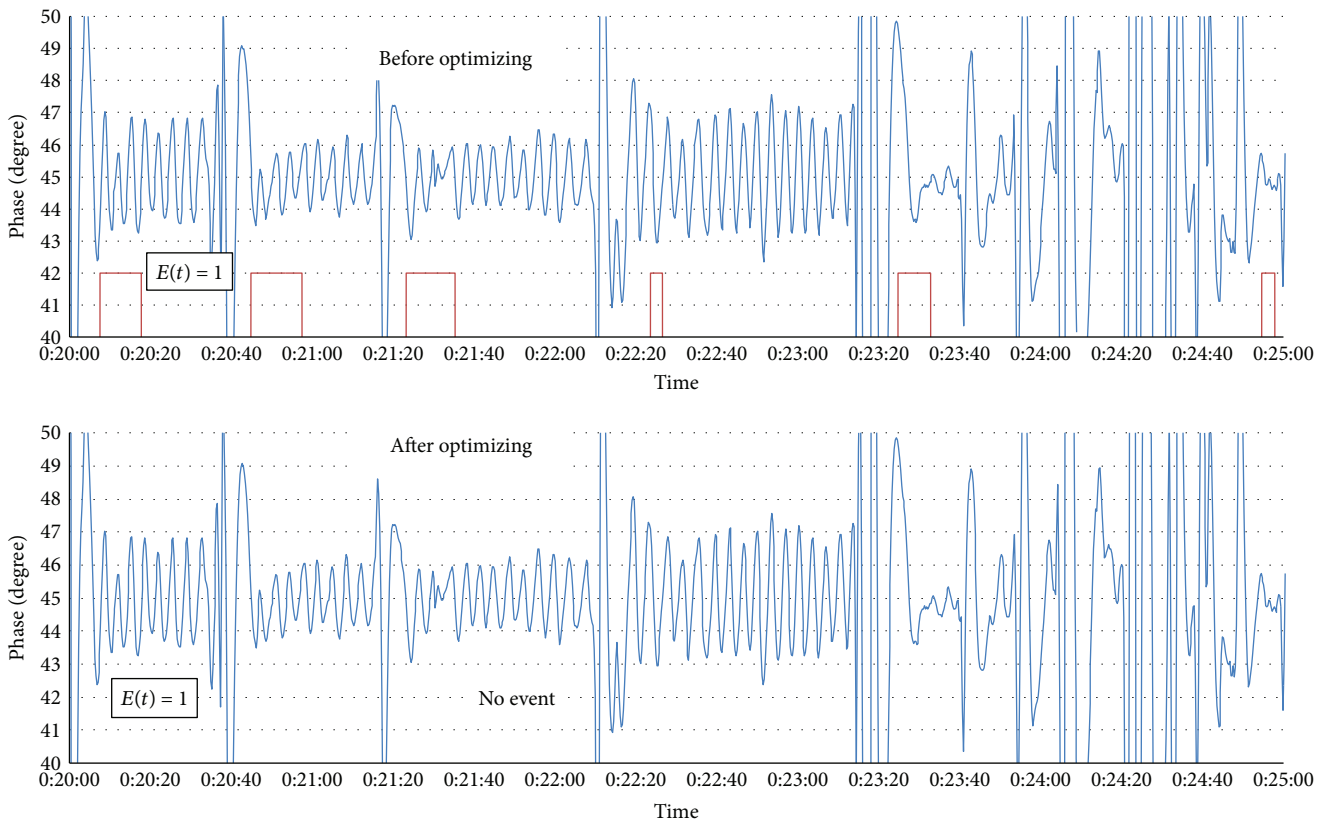

Figure 3: Typical sample of body movement noises, before optimizing and after optimizing. Body-movement-like noises are eliminated. AHI = 14 participants.

value of 1.0 yielded the best results. The optimized K value was incorporated into the software used for analysis of patient data. During measurement, the hypopnea threshold is automatically updated by the minute to achieve high sensitivity and specificity.

3. Results

A representative data sample from a patient with normal respiration is presented in Figure 2. In this case, no hypopnea events have been identified, and $E(t)$ is always equal to 0. Figure 3 includes data from a patient with strong body movement both prior to and following optimization. Figure 4 presents pre- and postoptimization data from a patient exhibiting both hypopnea and body movement (AHI = 14). As shown in Figures 3 and 4, the automatic hypopnea threshold optimizer effectively reduced noise associated with body movement: Figure 3 depicts the elimination of six events associated with body movement. As there were no events during this period, $E(t)$ was always equal to 0. In Figure 4,

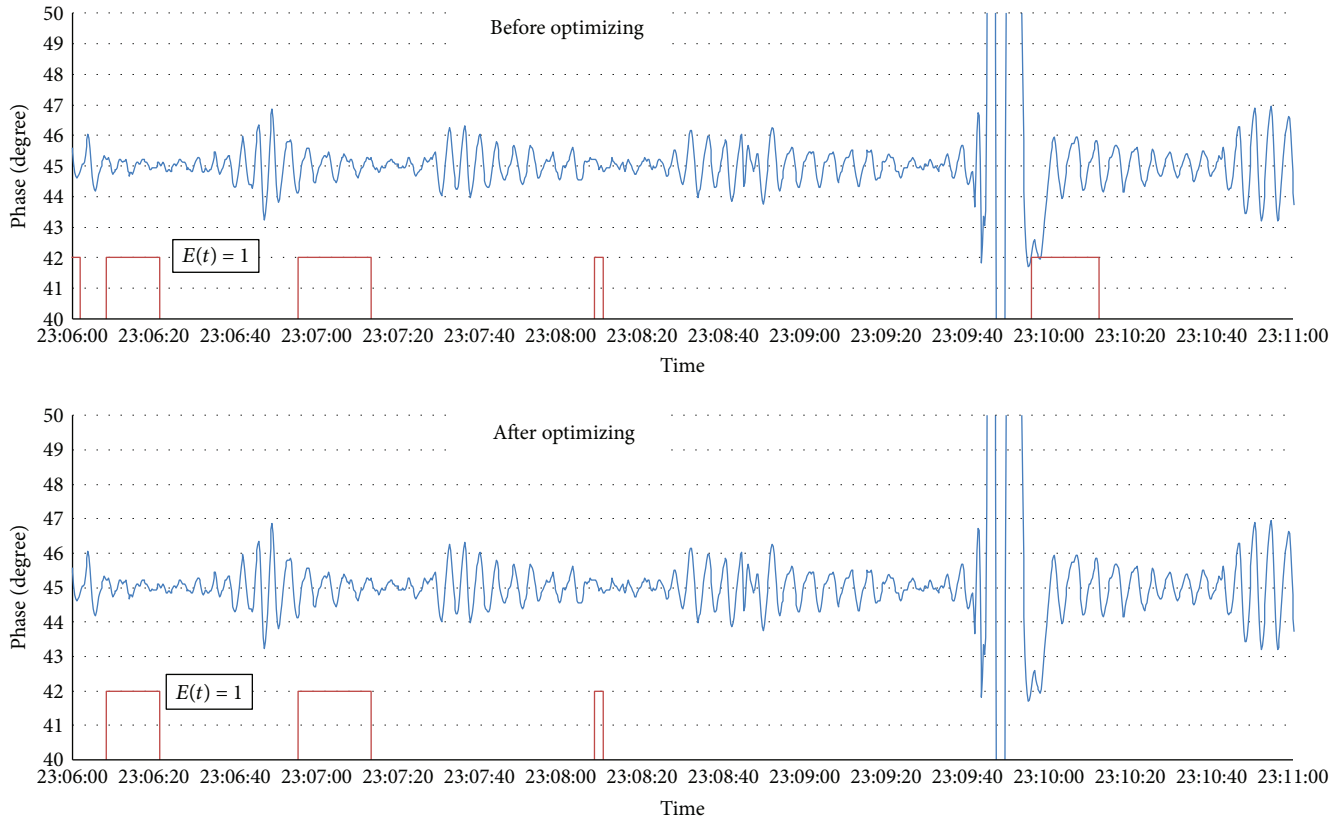

Figure 4: Hypopnea and body-movement noise in a single patient. After optimization, only body-movement-like events have been eliminated. AHI = 14.

frequent hypopnea events and one large deviation due to body movement can be observed, resulting in the generation of four events. Following optimization, noise associated with the body movement event had been eliminated, although the three hypopnea events remained. These findings indicate that the automatic hypopnea threshold optimizer effectively eliminated noise associated with body movement. The individual mean amplitude values for all participants are summarized in Table 1. Mean values were calculated separately for each radar system. As shown in Table 1, the numbers of radar detected events unproportionally increased along with K value. Average radar amplitudes of dual radars were weakly correlated with AHIs ($r = 0.51$ (radar1), $r = 0.52$ (radar2)).

ROC analysis was utilized to determine the appropriate K value prior to clinical testing. Only $K = 1.0$ yielded sensitivity and specificity values of 100%. The results of ROC analysis before and after optimization are presented in Figures 5(a)–5(d). Figures 5(a) and 5(c) represent the analysis using an AHI cutoff of 30, while Figures 5(b) and 5(d) represent the analysis using an AHI cutoff of 15.

When $K = 1.0$ and predictions of SAHS severity were based on an AHI > 30/h on PSG, the proposed system achieved a sensitivity of 100% and a specificity of 100%. Under the same conditions without optimization, sensitivity and specificity were 92% and 93%, respectively. Our findings further revealed that the number of events detected via radar can be approximated by multiplying the number of apnea-hypopnea events per hour by two-thirds. Thus, an AHI > 30/h is equivalent to >20 radar events per hour.

4. Discussion

In the present study, we aimed to develop a stand-alone screening system for the elimination of body movement artifacts based on automatic optimization of the apnea-hypopnea threshold. Notably, we calculated the average amplitude of respiration for the full duration of sleep, while previous studies have utilized the mean value obtained from a small sample of sleep data in which respiration remained stable. However, this method of determining the individual patient's baseline value is problematic, as the resulting values cannot account for changes in sleep stage, arousal, and posture. Kagawa et al. [16] also used an amplitude-based detection method; they utilized 40 s of normal-amplitude data to determine the individual baseline, setting the thresholds for apnea and hypopnea to 20% and 70%, of baseline, respectively. Using this method, Kagawa et al. achieved sensitivity and specificity values of 90% and 79%, respectively, for predicting the severity of SAHS based on an apnea-hypopnea index (AHI) of >30/h. However, our automatic optimization method yielded much higher sensitivity and specificity of 100% and 100%, respectively.

Our findings indicate that more stable measurements can be obtained by calculating the mean for the total duration of sleep.

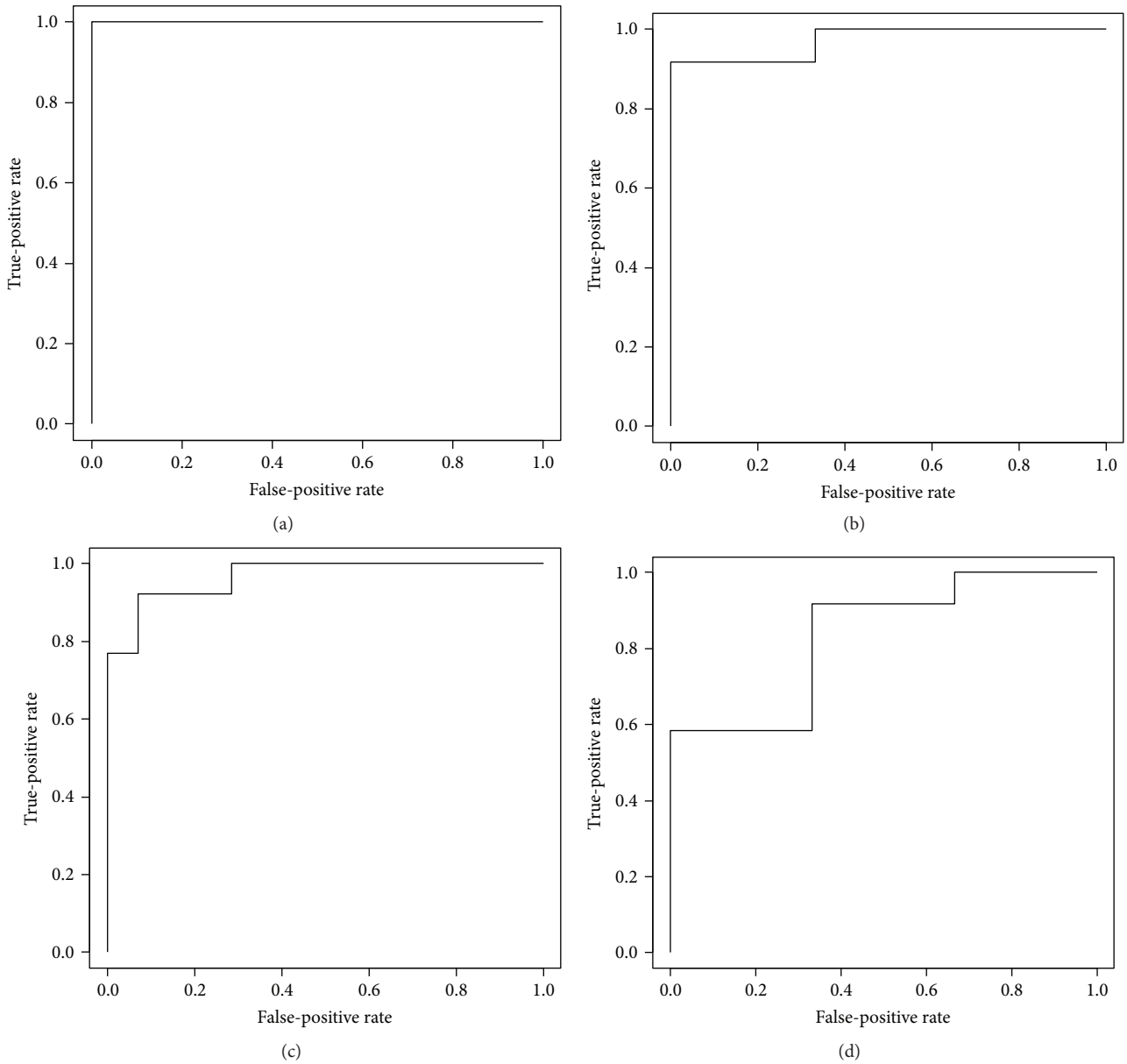

Figure 5: ROC curve ($K = 1.0$). Panel (a) presents an AHI > 30 positive case, after optimization. Panel (b) presents an AHI > 15 positive case, after optimization. Panel (c) presents an AHI > 30 positive case, before optimization. Panel (d) presents an AHI > 15 positive case, before optimization. All charts were made using R software.

Furthermore, we determined the optimum K value via ROC analysis. Although the appropriate K value was lower than expected, our findings indicated that the proposed method was effective in the screening and diagnosis of patients with SAHS. Our findings suggest that respiration data exhibit relatively small changes in overall amplitude and that interference caused by body movement produces large spikes in amplitude, which can be eliminated using a small K value of 1. However, as the present study included a small number of participants, further studies involving larger patient samples are required to determine the mechanisms underlying this effect. Furthermore, all participants of the present study had been diagnosed with SAHS. As such, future studies should include a control group of healthy participants to improve the generalizability of our findings.

5. Conclusion

The results of the present study indicate that measurement of respiration during sleep can be accomplished using radar-based systems equipped with an automatic hypopnea threshold optimizer. Moreover, our findings indicate that such noninvasive, stand-alone, and contact-free measurement can be used to screen for SAHS in patient homes and in more varied clinical settings. Such devices may reduce the incidence of serious complications associated with SAHS

and other sleep disorder and reduce medical costs due to misdiagnosis of sleep disorders.

Conflicts of Interest

The authors declare that there are no conflicts of interest regarding the publication of this article.

Acknowledgments

This study was supported in part by the 2013–2015 "Growth, Industry, Innovation" project of the Kanagawa Prefectural Government.

References

[1] T. Young, M. Palta, J. Dempsey, J. Skatrud, S. Weber, and S. Badr, "The occurrence of sleep-disordered breathing among middle-aged adults," *The New England Journal of Medicine*, vol. 328, no. 17, pp. 1230–1235, 1993.

[2] J. C. Lin, "Microwave sensing of physiological movement and volume change: a review," *BioElectroMagnetics*, vol. 13, no. 6, pp. 557–565, 1992.

[3] I. Arai, K. Motomura, and T. Suzuki, "A microwave Doppler radar system for noncontact measurement of head and finger movements in clinical use," *IEICE Transactions on Communications*, vol. E76B, no. 10, pp. 1318–1324, 1993.

[4] D. Dei, G. Grazzini, G. Luzi et al., "Noncontact detection of breathing using a microwave sensor," *Sensors*, vol. 9, no. 4, pp. 2574–2585, 2009.

[5] W. Massagram, V. M. Lubecke, and O. Boric-Lubecke, "Microwave non-invasive sensing of respiratory tidal volume," in *2009 Annual International Conference of the IEEE Engineering in Medicine and Biology Society*, pp. 4832–4835, Minneapolis, MN, USA, 2009.

[6] J.-H. Oum, D.-W. Kim, and S. Hong, "Two frequency radar sensor for non-contact vital signal monitor," in *2008 IEEE MTT-S International Microwave Symposium Digest*, pp. 919–922, Atlanta, GA, USA, USA, 2008.

[7] T. Matsui, S. Gotoh, I. Arai et al., "Noncontact vital sign monitoring system for isolation unit (casualty care system)," *Military Medicine*, vol. 171, no. 7, pp. 639–643, 2006.

[8] A. D. Droitcour, T. B. Seto, B. Park et al., "Non-contact respiratory rate measurement validation for hospitalized patients," in *2009 Annual International Conference of the IEEE Engineering in Medicine and Biology Society*, pp. 4812–4815, Minneapolis, MN, USA, 2009.

[9] I. Arai, "Survivor search radar system for persons trapped under earthquake rubble," in *APMC 2001. 2001 Asia-Pacific Microwave Conference (Cat. No.01TH8577)*, pp. 663–668, Taipei, Taiwan, Taiwan, 2001.

[10] "Japan Patent Office; patent publication," JP 3700-00954A, 2005.

[11] S. Suzuki, T. Matsui, H. Kawahara et al., "A non-contact vital sign monitoring system for ambulances using dual-frequency microwave radars," *Medical & Biological Engineering & Computing*, vol. 47, no. 1, pp. 101–105, 2009.

[12] S. Gotoh, T. Matsui, H. Imuta, M. Kagawa, Z. Badarch, and T. Matsui, "Non-contact determination of parasympathetic activation induced by a full stomach using microwave radar," *Medical & Biological Engineering & Computing*, vol. 47, no. 9, pp. 1017–1019, 2009.

[13] S. Gotoh, T. Matsui, K. Yamashita et al., "A study for novel non-contact sleep respiration disorder measuring system utilizing micro-wave radar and application to screening of sleep apnea syndrome and other sleep respiratory disorder," *Iryou kikigaku (The Japanese journal of medical instrumentation)*, vol. 84, no. 3, pp. 317–324, 2014.

[14] S. Gotoh, T. Matsui, M. Kojima, K. Yamashita, and Y. Sakamoto, "Comparison study between micro wave radar and conventional SpO_2 measurement for primary screening of sleep apnea syndrome," *Journal of Life Support Engineering*, vol. 26, no. 4, pp. 126–131, 2014.

[15] S. Gotoh, T. Matsui, K. Yamashita, H. Kaneko, Y. Naka, and O. Kurita, "A clinical study for non-contact sleep respirometry with microwave radar, monitored by simultaneous measuring with polysomnography," *Iryou kikigaku (The Japanese journal of medical instrumentation)*, vol. 86, no. 5, pp. 441–449, 2016.

[16] M. Kagawa, H. Tojima, and T. Matsui, "Non-contact diagnostic system for sleep apnea-hypopnea syndrome based on amplitude and phase analysis of thoracic and abdominal Doppler radars," *Medical & Biological Engineering & Computing*, vol. 54, no. 5, pp. 789–798, 2016.

[17] M. Kagawa, Y. Yoshida, M. Kubota, A. Kurita, and T. Matsui, "Non-contact heart rate monitoring method for elderly people in bed with random body motions using 24 GHz dual radars located beneath the mattress in clinical settings," *Journal of Medical Engineering & Technology*, vol. 36, no. 7, pp. 344–350, 2012.

[18] M. Kagawa, K. Ueki, H. Tojima, and T. Matsui, "Noncontact screening system with two microwave radars for the diagnosis of sleep apnea-hypopnea syndrome," in *2013 35th Annual International Conference of the IEEE Engineering in Medicine and Biology Society (EMBC)*, pp. 2052–2055, Osaka, Japan, 2013.

[19] L. Anishchenko, G. Gennarelli, A. Tataraidze, E. Gaysina, F. Soldovieri, and S. Ivashov, "Evaluation of rodents' respiratory activity using a bioradar," *IET Radar, Sonar & Navigation*, vol. 9, no. 9, pp. 1296–1302, 2015.

[20] M. Baboli, A. Singh, B. Soll, O. Boric-Lubecke, and V. M. Lubecke, "Good night: sleep monitoring using a physiological radar monitoring system integrated with a polysomnography system," *IEEE Microwave Magazine*, vol. 16, no. 6, pp. 34–41, 2015.

[21] L. Zhang, J. Xiong, H. Zhao, H. Hong, X. Zhu, and C. Li, "Sleep stages classification by CW Doppler radar using bagged trees algorithm," in *2017 IEEE Radar Conference (RadarConf)*, pp. 0788–0791, Seattle, WA, USA, 2017.

[22] Z. T. Beattie, T. L. Hayes, C. Guilleminault, and C. C. Hagen, "Accurate scoring of the apnea–hypopnea index using a simple non-contact breathing sensor," *Journal of Sleep Research*, vol. 22, no. 3, pp. 356–362, 2013.

[23] B. Razavi, "Design consideration for direct-conversion receivers," *IEEE Transactions on Circuits and Systems II: Analog and Digital Signal Processing*, vol. 44, no. 6, pp. 428–435, 1997.

[24] G. Gennarelli, F. Soldovieri, L. Marciano, G. Cerasuolo, and O. Petrella, "Measurements performance of a bioradar for human respiration monitoring," *Procedia Engineering*, vol. 168, pp. 1200–1203, 2016.

[25] R. B. Berry, R. Budhiraja, D. J. Gottlieb et al., "Rules for scoring respiratory events in sleep: update of the 2007 AASM manual for the scoring of sleep and associated events. Deliberations of the sleep apnea definitions task force of the American Academy of Sleep Medicine," *Journal of Clinical Sleep Medicine*, vol. 8, no. 5, pp. 597–619, 2012.

Hindawi
Journal of Sensors
Volume 2017, Article ID 3738046, 7 pages
https://doi.org/10.1155/2017/3738046

Research Article

Thermal Sensor Circuit Using Thermography for Temperature-Controlled Laser Hyperthermia

Shinsuke Nomura,[1] Masashi Arake,[2] Yuji Morimoto,[2] Hironori Tsujimoto,[1] Hiromi Miyazaki,[3] Daizoh Saitoh,[3] Nariyoshi Shinomiya,[2] Kazuo Hase,[1] Junji Yamamoto,[1] and Hideki Ueno[1]

[1]*Department of Surgery, National Defense Medical College, Tokorozawa, Japan*
[2]*Department of Integrative Physiology and Bio-Nano Medicine, National Defense Medical College, Tokorozawa, Japan*
[3]*Division of Traumatology, National Defense Medical College Research Institute, Tokorozawa, Japan*

Correspondence should be addressed to Yuji Morimoto; moyan@ndmc.ac.jp

Received 9 June 2017; Revised 19 August 2017; Accepted 29 August 2017; Published 9 October 2017

Academic Editor: Guanghao Sun

Laser hyperthermia is a powerful therapeutic modality that suppresses the growth of proliferative lesions. In hyperthermia, the optimal temperature range is dependent on the disease; thus, a temperature-driven laser output control system is desirable. Such a laser output control system, integrated with a thermal sensor circuit based on thermography, has been established. In this study, the feasibility of the developed system was examined by irradiating mouse skin. The system is composed of a thermograph, a thermal sensor circuit (PC and microcontroller), and an infrared laser. Based on the maximum temperature in the laser-irradiated area acquired every 100 ms during irradiation, the laser power was controlled such that the maximum temperature was maintained at a preset value. Temperature-controlled laser hyperthermia using the thermal sensor circuit was shown to suppress temperature fluctuations during irradiation (SD ~ 0.14°C) to less than 1/10 of those seen without the thermal sensor circuit (SD ~ 1.6°C). The thermal sensor circuit was able to satisfactorily stabilize the temperature at the preset value. This system can therefore provide noncontact laser hyperthermia with the ability to maintain a constant temperature in the irradiated area.

1. Introduction

Laser hyperthermia (LH) is a promising and minimally invasive therapy used in various medical fields. The therapeutic indications of LH include superficial lesions such as neoplasm [1], plantar warts [2], condyloma acuminata [3], or human papillomavirus-infected skin [4]. In the field of orthopedic surgery, it has been reported that LH promotes bone healing for fractures and is suitable for treating osteoarthritis [5, 6].

When using LH, it is important to control the heating in order to keep the temperature of a lesion within the particular thermal range that induces the maximum therapeutic effect. For this reason, various devices for temperature monitoring during LH have been developed [7, 8], including thermocouples [8], thermistors [9], and infrared temperature monitors [10]. Most of these temperature monitoring devices, however, only provide one value for the average temperature in a certain area. When the whole area of a target lesion is heated, the increases in temperature in small subdivided regions within the whole area are not always equal. This is because biological tissue is generally composed of small structures, each of which has different thermal characteristics. Such situations are likely to cause unintended effects during LH, such as excessive local heating due to the spatial irregularity of the lesion. This strongly suggests that temperature monitoring devices that only show "one value" temperature information are insufficient for monitoring the heating status during LH.

One solution to this limitation is to use thermal imaging (thermography) that can obtain individual temperatures in subdivided small areas within the whole area of a target lesion. However, thermography has rarely been used as the temperature monitoring device for LH. In addition, to our

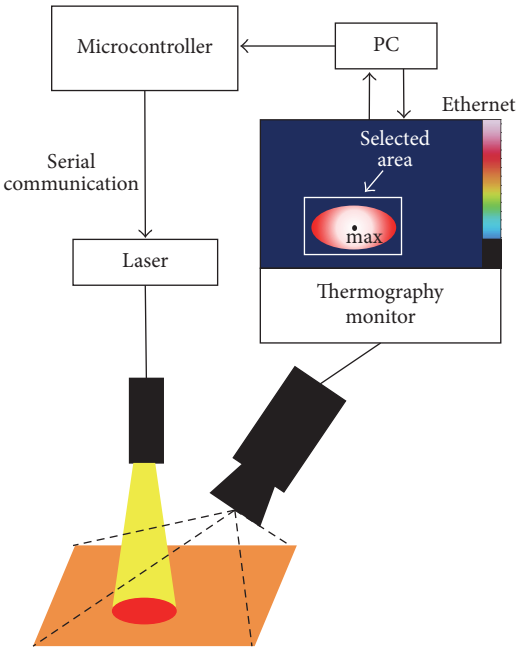

Figure 1: Schematic diagram of the thermal sensor circuit using thermography for laser hyperthermia. PC: personal computer.

knowledge, there are few examples where thermography has been used for temperature control in LH [11]. Therefore, an LH system using thermography has been developed, which provides feedback from each temperature in several subdivided small areas within the whole area of a target lesion to the laser output control unit (patent number: PCT/JP2016/079124).

The aim of this study is to examine the feasibility of this thermography-based thermal sensor circuit for temperature-controlled LH, using the skin of small animals.

2. Materials and Methods

2.1. Animals. Two different representative species of *Mus musculus* (BALB/c and C57BL/6), which are often used as laboratory animals, were selected, as the effect of the laser might differ depending on the type of mice. Female BALB/c Cr mice at 6 weeks of age (Japan SLC, Hamamatsu, Japan) and C57BL/6 mice at 6 weeks of age (Japan SLC, Hamamatsu, Japan) were fed under specific pathogen-free conditions. All animal procedures were performed in accordance with the guidelines approved by the National Defense Medical College Animal Care and Use Committee.

Hairs from the mice were removed one day before laser irradiation; hairs on the right dorsal skin were roughly cut with a clipper and were completely removed using a hair removal cream. The laser irradiation experiment with a thermal sensor circuit (described below) was carried out using one mouse of each species, and the laser irradiation experiment without the thermal sensor circuit (described below) was performed using three mice from each species.

2.2. Near-Infrared Irradiation and Thermal Dosimetry Settings. A fiber-coupled laser diode emitting an 808 nm laser (model FC-W-808, maximum output: 10 W; Changchun New Industries Optoelectronics Technology Co., Ltd., Jilin, China) was used as the LH device. The fiber probe was placed above the dorsal skin of the mice such that the irradiated area was 0.20 cm^2 (diameter = 0.5 cm). The skin temperature was measured using a high-resolution infrared thermograph (FSV-2000, Apiste Corporation, Osaka, Japan). The maximum frame rate of the thermograph is 50 fps, the temperature accuracy is ±2%, and the spatial resolution is 384 × 288 pixels. From the whole area of pixels within an arbitrarily selected region, this thermograph automatically detects both maximum temperature and minimum temperature every 20 ms.

2.3. Structure of the Thermal Sensor Circuit and the Temperature Control System. In order to keep the skin temperature constant, the laser power was automatically adjusted by a thermograph-based thermal sensor circuit (Figure 1). Multipoint temperatures in a selected area including the irradiated spot were captured by the thermal sensor circuit and transmitted to a PC. A microcontroller connected to the PC modulated the laser current, the magnitude of which was controlled in the following manner: the target temperature (tar(T)) that we aim to maintain in the heating area was input into the program that controls the thermal sensor circuit. In this experiment, the laser current started at 9.2 A, which corresponded to a laser output of approximately 1.8 W/cm^2. The upper limits of the laser current were set to 11.2 A (corresponding to 7 W/cm^2). All initial setting values were provisional and could have been changed arbitrarily. The

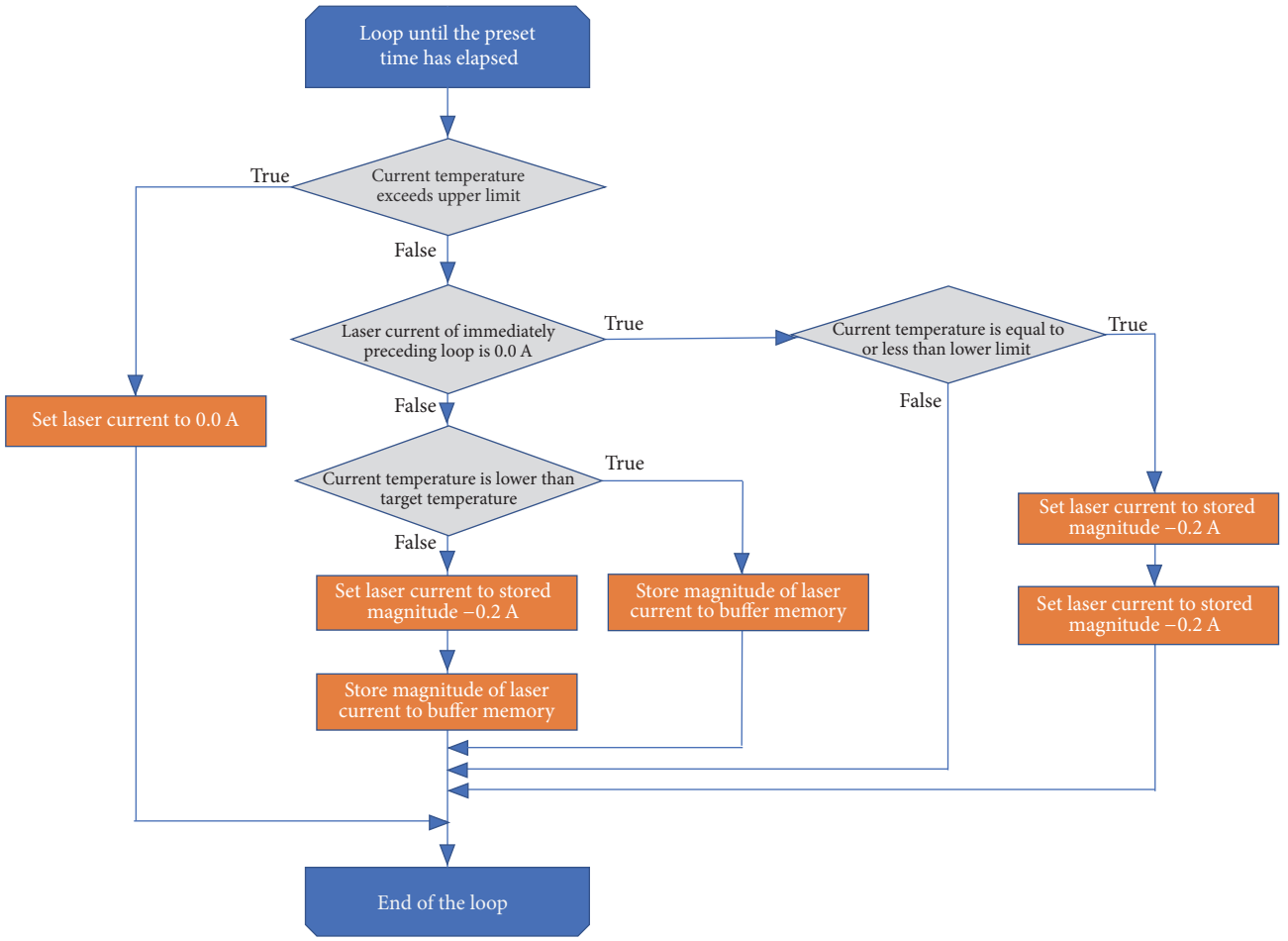

Figure 2: Flowchart of laser current adjustment based on temperature.

workflow of the program for the thermal sensor circuit obeyed the flowchart shown in Figure 2. The total processing time, including temperature sampling, output control, and laser irradiation, was 100 ms. Since the rise and fall durations of the infrared laser are 1 μs each, they did not affect the controlled period (100 ms). Typical adjustment of the laser current based on the acquired maximum temperature is described below.

For this case, the upper and lower limits were set to ±0.1°C of tar(T). At 1 s after the initiation of the laser irradiation, when the acquired maximum temperature had not reached tar(T), the laser current was increased to 11.2 A. Thereafter, when the acquired maximum temperature exceeded tar(T) by 0.1°C or more, the laser current was dropped to 0 A. Then, when the acquired maximum temperature was less than tar(T) by 0.1°C, the laser current was adjusted to 0.2 A below the last current value immediately before the current was turned off. When the acquired maximum temperature was still lower than tar(T), the laser current was adjusted to a value 0.2 A higher than the value 100 ms before. The variation in the current (±0.2 A) was ascribed to the functional limitation of the laser equipment used. In the stable phase, in which the time-dependent variation in the acquired maximum temperatures was small, the laser current was gradually decreased and then repeatedly turned on and off at a certain constant value.

2.4. Laser Irradiation Protocol. Mice were placed in the left lateral decubitus position and the dorsal skin was irradiated using the laser system. The camera (FSV-210L, Apiste) of the thermograph was fixed so that the long axis of the camera was parallel to that of the laser beam. The zoom lens (FSV-L212, Apiste) was adjusted so that all of the skin of the right back of the mouse was included in the monitor view. A target region for measuring the temperature was determined so as to cover the whole area of the irradiation spot (Figure 1). Regardless of the use of the thermal sensor circuit, an area of the selected target region was set at a fixed value, resulting in a 96 × 72 pixel area (corresponding to 29 mm × 22 mm in a real area of the skin). As mentioned previously, the maximum temperature within the whole selected region was automatically detected every 20 ms.

2.4.1. Laser Irradiation Using a Thermal Sensor Circuit. The right dorsal skin of the mouse was irradiated with the laser for 300 s using the thermal sensor circuit system, setting tar(T)

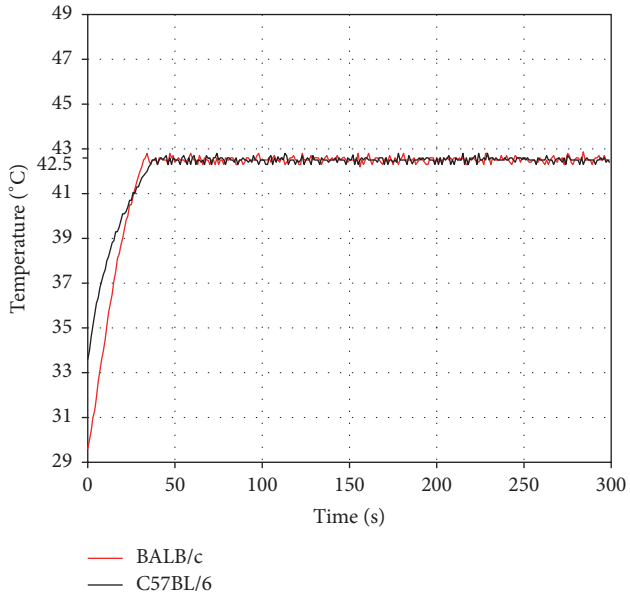

Figure 3: Temperature changes on the skin of the BALB/c mouse *(red line)* and C57BL/6 mouse *(black line)* under laser irradiation with the thermal sensor circuit.

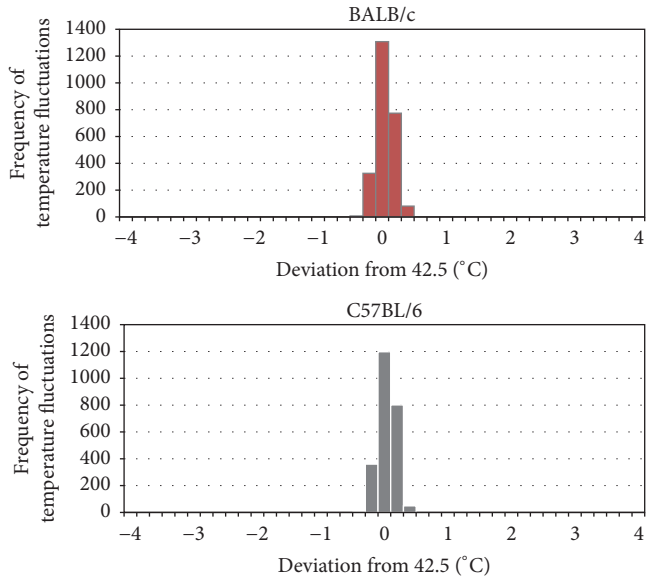

Figure 4: Frequency distribution of temperature fluctuations: a fluctuation was defined as the difference between tar(T) = 42.5°C and the maximum temperature in the selected area, and the maximum temperature was acquired every 100 ms.

at 42.5°C. Photographs of the irradiated skin were obtained two days after the irradiation, when the pathological dermal changes (i.e., burn blisters) are usually most prominent.

2.4.2. Laser Irradiation without a Thermal Sensor Circuit. The right dorsal skin of a mouse was irradiated with the laser at a constant power density of 6 W/cm^2 for 300 s, while monitoring and recording the highest temperature within the selected area using thermography. Photographs of the irradiated skin were obtained two days after the irradiation.

3. Results

The laser output control system integrated with the thermal sensor circuit using thermography succeeded in keeping the temperature at the target area constant during laser irradiation, even with different types of mice (Figure 3). Once the temperature reached the tar(T) (*X*, 42.5°C) after the initiation of laser irradiation (approximately 40 s after the irradiation), the average temperature of the BALB/c mouse and C57BL/6 mouse was 42.52°C and 42.51°C, respectively, with standard deviations of 0.14°C and 0.14°C (Figure 3). The temperature value every 100 ms after reaching the tar(T) of 42.5°C was within the range of 42.5 ± 0.1°C for 52.53% of the time for the BALB/c mouse and 49.71% of the time for the C57BL/6 mouse (Figure 4).

On the other hand, in the case of laser irradiation without the thermal sensor circuit, the temperature of the target area was not stabilized (Figure 5). When compared at 40 s after the laser irradiation, the average temperatures of the BALB/c mice and C57BL/6 mice were 44.01°C and 43.60°C, respectively, with standard deviations of 1.74°C and 1.58°C (Figure 5 and Table 1). The skin temperature of one of the

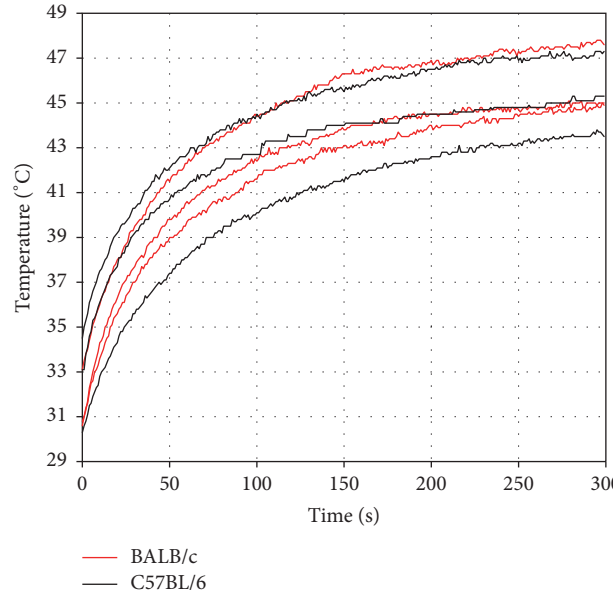

Figure 5: Temperature changes on the skin of BALB/c mice *(red lines)* and C57BL/6 mice *(black lines)* under laser irradiation without the thermal sensor circuit. In this case, the power density of the laser was fixed at 6 W/cm^2.

BALB/c mice (number 3) exceeded 47°C, and the animal showed blister formation corresponding to the irradiated area, suggesting the occurrence of a first-degree burn (Figure 6(a)). Histopathological examination (Hematoxylin and Eosin stain) of the BALB/c mouse (number 3) revealed that the squamous epithelium was not seen in the irradiated area, which is consistent with a first-degree burn (Figure 7). All of

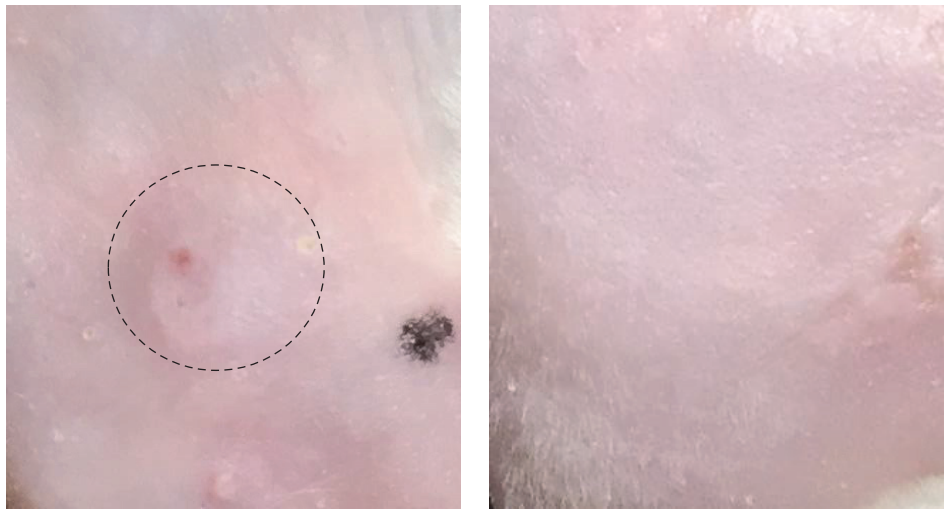

(a) (b)

Figure 6: Photographs of the skin two days after irradiation with a fixed power density (6 W/cm^2). (a) BALB/c mouse number 3; bubbles were seen in the skin *(dotted circle line)*. (b) BALB/c mouse number 2; no change was seen in the skin.

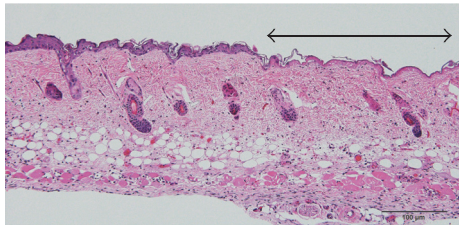

Figure 7: Microscopic image of the skin corresponding to Figure 6(a) (BALB/c mouse number 3), marked using Hematoxylin and Eosin stain. Loss of the squamous epithelium is seen *(both ends of arrow)* in the area of the laser-irradiated spot.

Table 1: The average value and standard deviation of the temperature sampling data every 100 ms from 40 seconds after the start of laser irradiation until the end of irradiation.

	Number	Max	Mean	SD	Mean	SD
BALB/c	(1)	45.10	42.83	1.77	44.01	1.74
	(2)	47.83	43.46	1.60		
	(3)	45.02	45.73	1.86		
C57BL/6	(1)	45.31	41.50	1.87	43.60	1.58
	(2)	47.34	43.75	1.31		
	(3)	43.83	45.56	1.55		

the other mice showed no obvious change in the irradiated skin (Figure 6(b)).

4. Discussion

The present study showed that temperature-controlled laser hyperthermia using the thermal sensor circuit exhibited excellence in maintaining a tar(T). Temperature-controlled laser hyperthermia using the thermal sensor circuit resulted in suppression of the temperature fluctuations during irradiation (SD ~ 0.14°C) to less than 1/10 of those seen without the thermal sensor circuit (SD ~ 1.6°C).

The degree of temperature increase due to the LH depends on several factors, such as the laser wavelength, power density of the laser, density of melanin pigment, distribution of capillaries in the epidermis, and concentration of hemoglobin in the blood [12, 13]. Therefore, it is important to monitor the temperature of the lesion during LH.

For effective LH, it is necessary to heat the lesion up to the tar(T); however, overheating the lesion should be avoided. Although the maximum temperature was around 45°C in most of the mice irradiated without the thermal sensor circuit, some of the mice bore low-temperature burn, as shown in Figure 6. Therefore, the tar(T) should be kept within an appropriate range. An optimal temperature range for LH is considered to be from 42°C to 45°C; this range promotes the migration and maturation of Langerhans cells [14], which activate immune responses.

Temperature-controlled systems using the combination of a hyperthermic apparatus and a noninvasive temperature monitor have been developed, and some of them have been used clinically [3, 7, 8, 10, 14–16]. A noncontact type thermal monitoring system, other than thermography, has also been reported [3, 10, 14]; however, it only shows one value for the average temperature in a certain area. In contrast, the present thermal sensor circuit is unique in its ability to acquire multipoint temperatures (thermal images) using thermograph.

There are several challenges to be addressed to advance the present system toward practical use in clinical applications. The first challenge is to verify the effectiveness of the thermal sensor circuit when applied to lesions such as tumors and plantar warts. Most of the neovessels in such lesions often show a poor vasodilating property; thus, the delivered

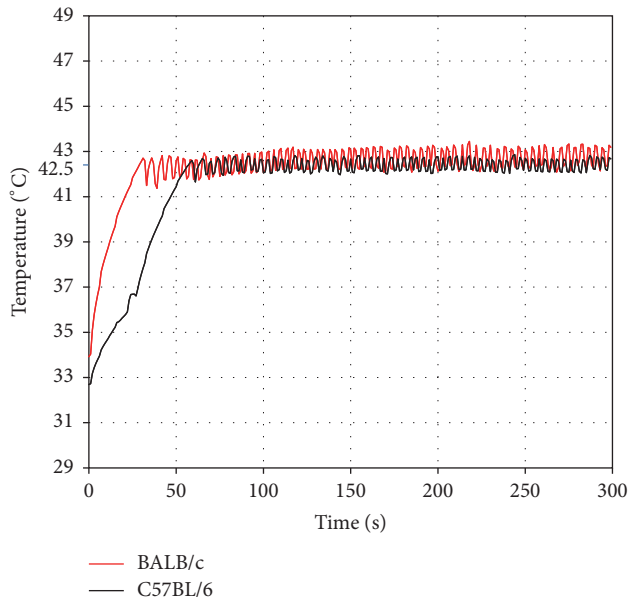

Figure 8

heat tends to be retained owing to insufficient blood flow, and the temperature of the lesions is liable to increase [17]. The second challenge is to improve the temperature control. The program that controlled the thermal sensor circuit in the present study was a simple modification of the on-off control method. Approximately 50% of the temperature values every 100 ms after reaching the tar(T) of 42.5°C were within the range of 42.5 ± 0.1°C. The use of other control methods may further suppress the temperature fluctuation. One candidate is the proportional-integral-derivative (PID) control method, which is reported to correct the fluctuation of temperature more tightly than the on-off control method [7, 18]. The third challenge is to establish a method for the estimation of the temperature inside an irradiated target from the surface temperature, since thermography in principle measures the surface-to-air temperature.

5. Conclusions

Our developed thermal sensor circuit using thermography for temperature-controlled LH successfully suppressed the temperature fluctuation during laser irradiation to less than 1/10 of that seen when compared to irradiation without the thermal sensor circuit.

Appendix

The thermal sensor circuit for temperature-controlled laser hyperthermia worked well in the case using thermography. However, thermography is only applicable for sensing the surface temperature of a heated object. Hence, to demonstrate the usefulness of the thermal sensor circuit even when sensing the interior temperature of a heated object, an additional experiment was performed using a thermocouple.

A needle-shaped thermocouple probe (HYP0, OMEGA Engineering Inc., Stamford, CT) combined with a data logger (TC08, Pico Technology, Cambridgeshire, UK) was used for measuring an intradermal temperature. The probe consists of an extremely small type T (copper-constantan) thermocouple implanted in a stainless steel needle (φ = 0.2 mm; length = 25 mm). The temperature accuracy is ±0.2%. Using the thermal sensor circuit, the intradermal temperature was automatically captured through the thermocouple every 100 ms.

The needle-shaped thermocouple probe was inserted into a mouse intradermally and was advanced so that the needle top (metal joint portion) was placed in the center of the laser irradiation field. One BALB/c mouse and one C57BL/6 mouse were used.

Even using the thermocouple probe, the thermal sensor circuit worked well and fulfilled the temperature-controlled laser hyperthermia. Once the temperature reached the target temperature (tar(T)) (X, 42.5°C) after the initiation of laser irradiation, the average temperatures of the BALB/c and C57BL/6 mice were 42.66°C and 42.41°C, respectively, with standard deviations of 0.45°C and 0.29°C (Figure 8). The temperature value captured every 100 ms after reaching the tar(T) of 42.5°C was within the range of 42.5±0.1°C for 14.13% of the time for the BALB/c mouse and 15.17% of the time for the C57BL/6 mouse.

The thermal sensor circuit worked well with an invasive temperature measuring device such as a thermocouple. However, in this case, the initial temperature rise was slower and the temperature fluctuation during the thermal-equilibrium phase was larger compared to those when using the thermograph. These findings suggest that, in the case of laser hyperthermia, the temperature control in deep lesions is accompanied by a large fluctuation in the temperature of the lesions when using an on-off type sensor circuit.

Conflicts of Interest

The authors report no proprietary or commercial conflicts of interest in any product mentioned or concept discussed in this article.

Authors' Contributions

Shinsuke Nomura and Masashi Arake have contributed equally to this work.

Acknowledgments

The authors would like to acknowledge Editage (https://www.editage.jp) for English language editing. This work was supported by the Japan Society for the Promotion of Science (Kakenhi) under Grant no. 17H02114.

References

[1] Y.-C. Yang, Y.-W. Cheng, C.-S. Lai, and W. Chen, "Prevalence of childhood acne, ephelides, warts, atopic dermatitis, psoriasis, alopecia areata and keloid in Kaohsiung County, Taiwan: A community-based clinical survey," *Journal of the European Academy of Dermatology and Venereology*, vol. 21, no. 5, pp. 643–649, 2007.

[2] Y. Ma, W. Huo, Y.-X. Hong, H.-D. Chen, and X.-H. Gao, "Successful clearance of facial common warts by local hyperthermia: Report of two cases," *Dermatologic Therapy*, vol. 25, no. 4, pp. 386–388, 2012.

[3] X. Wang, X.-H. Gao, X. Li et al., "Local hyperthermia induces apoptosis of keratinocytes in both normal skin and condyloma acuminata via different pathways," *Apoptosis*, vol. 14, no. 5, pp. 721–728, 2009.

[4] X. Gao and H. Chen, "Hyperthermia on skin immune system and its application in the treatment of human papillomavirus-infected skin diseases," *Frontiers of Medicine in China*, vol. 8, no. 1, pp. 1–5, 2014.

[5] J. Son, Y.-B. Kim, Z. Ge, S.-H. Choi, and G. Kim, "Bone healing effects of diode laser (808 nm) on a rat tibial fracture model," *in vivo*, vol. 26, no. 4, pp. 703–709, 2012.

[6] J. Y. Lee, S. U. Lee, T. Lim, and S. H. Choi, "Healing effects and superoxide dismutase activity of diode/Ga-As lasers in a rabbit model of osteoarthritis," *In Vivo*, vol. 28, no. 6, pp. 1101–1106, 2014.

[7] X. Feng, F. Gao, C. Xu, L. Gaoming, and Y. Zheng, "Self temperature regulation of photothermal therapy by laser-shared photoacoustic feedback," *Optics Letters*, vol. 40, no. 19, pp. 4492–4495, 2015.

[8] T. H. Nguyen, S. Park, K. K. Hlaing, and H. W. Kang, "Temperature feedback-controlled photothermal treatment with diffusing applicator: theoretical and experimental evaluations," *Biomedical Optics Express*, vol. 7, no. 5, pp. 1932–1947, 2016.

[9] K. Ivarsson, L. Myllymäki, K. Jansner, U. Stenram, and K.-G. Tranberg, "Resistance to tumour challenge after tumour laser thermotherapy is associated with a cellular immune response," *British Journal of Cancer*, vol. 93, no. 4, pp. 435–440, 2005.

[10] W. Huo, X.-H. Gao, X.-P. Sun et al., "Local hyperthermia at 440◦c for the treatment of plantar warts: a randomized, patient-blinded, placebo-controlled trial," *Journal of Infectious Diseases*, vol. 201, no. 8, pp. 1169–1172, 2010.

[11] S. A. Shevchik, G. V. Zhukov, I. N. Golovanov, K. G. Linkov, V. V. Barun, and V. B. Loschenov, "Temperature control technique for laser hyperthermia," in *Proceedings of the Advanced Biomedical and Clinical Diagnostic Systems VI*, usa, January 2008.

[12] J. Ortonne, "Photoprotective properties of skin melanin," *British Journal of Dermatology*, vol. 146, no. s61, pp. 7–10, 2002.

[13] B. S. Kwak, B. S. Kim, S.-H. Song, H. O. Kim, H. H. Cho, and H.-I. Jung, "Direct measurement of the in vitro hemoglobin content of erythrocytes using the photo-thermal effect of the heme group," *Analyst*, vol. 135, no. 9, pp. 2365–2371, 2010.

[14] X. Li, X.-H. Gao, L. Jin et al., "Local hyperthermia could induce migrational maturation of Langerhans cells in condyloma acuminatum," *Journal of Dermatological Science*, vol. 54, no. 2, pp. 121–123, 2009.

[15] K. Arunachalam, P. F. Maccarini, and P. R. Stauffer, "A thermal monitoring sheet with low influence from adjacent waterbolus for tissue surface thermometry during clinical hyperthermia," *IEEE Transactions on Biomedical Engineering*, vol. 55, no. 10, article no. 12, pp. 2397–2406, 2008.

[16] X.-h. Gao, D. Gao, X.-P. Sun et al., "Non-ablative controlled local hyperthermia for common warts," *Chinese Medical Journal*, vol. 122, no. 17, pp. 2061–2063, 2009 (English).

[17] A. Chicheł, J. Skowronek, M. Kubaszewska, and M. Kanikowski, "Hyperthermia - Description of a method and a review of clinical applications," *Reports of Practical Oncology and Radiotherapy*, vol. 12, no. 5, pp. 267–275, 2007.

[18] L. Sun, C. M. Collins, J. L. Schiano, M. B. Smith, and N. B. Smith, "Adaptive real-time closed-loop temperature control for ultrasound hyperthermia using magnetic resonance thermometry," *Concepts in Magnetic Resonance Part B: Magnetic Resonance Engineering*, vol. 27, no. 1, pp. 51–63, 2005.

Hindawi
Journal of Sensors
Volume 2017, Article ID 6486891, 7 pages
https://doi.org/10.1155/2017/6486891

Research Article

Detection of Stress Hormone in the Milk for Animal Welfare Using QCM Method

Takeshi Ito,[1] Nobuyoshi Aoki,[2] Akihisa Tsuchiya,[2] Satoru Kaneko,[2] Kiyoshi Akiyama,[3] Katsuji Uetake,[4] and Koji Suzuki[5]

[1]*Faculty of Engineering Science, Kansai University, Yamate-cho 3-3-35, Suita, Osaka 564-8680, Japan*
[2]*Kanagawa Institute of Industrial Science and Technology, Shimo-imaizumi 705-1, Ebina, Kanagawa 243-0435, Japan*
[3]*Livestock Industry Technology Station, Hongo 3750, Ebina, Kanagawa 243-0417, Japan*
[4]*School of Veterinary Medicine, Azabu University, Fuchinobe 1-17-71, Chuo, Sagamihara 252-5201, Japan*
[5]*Faculty of Science and Technology, Keio University, Hiyoshi 3-14-1, Kohoku, Yokohama 223-8522, Japan*

Correspondence should be addressed to Takeshi Ito; t.ito@kansai-u.ac.jp

Received 16 May 2017; Accepted 10 July 2017; Published 17 September 2017

Academic Editor: Takemi Matsui

We developed a rapid and sequential analysis system to determine stress marker in the milk. One of the famous stress markers, cortisol, was detected using our method. Quartz crystal microbalance (QCM) method with a twin sensor was used in this study. One channel detected stress marker corresponding to antigen-antibody interaction and the other channel was used as a reference to remove environmental influences. Although nonspecific adsorption was monitored on each channel, frequency difference between them was within a few Hz on the injection of sample solution. One determination cycle including regeneration step could be performed within 10 minutes. The system could detect the cortisol level from 0.1 pg/mL to 100 pg/mL. These results show that our system has a potential to check the daily feeding condition for cows in terms of animal welfare.

1. Introduction

Many biomarkers exist in biological fluid, for example, blood, urine, saliva, and milk. To assess daily health condition, noninvasive monitoring method of biomarker is desired for not only human but also animals. Animals including human face many stressors by life environments and physiological problems. Long-term and strong stress might cause not only mental diseases such as depression but also heart disease and high blood pressure for human. Animals also feel stress; for example, stress hormone level of abandonment dogs in Fukushima was 5 to 10 times larger than that in other areas in Japan after the big earthquake of March 11, 2011 [1].

Animal welfare is recently focussed in the livestock industry [2–5]. Controlling the stress level of farm animals is important not only in ethical concerns but also in high-quality production. Farm animals face many stressors around the feeding environment such as temperature, feed, and the number of animals per unit area. We focussed on a cow for an actual case. Cortisol is well known as a stress marker of the endocrine system. Some reports monitored cortisol level in cow's blood [6–9], and the concentration of cortisol was lower than 20 ng/mL. However, collecting blood is stressful for animals and controller. Noninvasive monitoring of cortisol level is desired for the daily stress test. Milk is ideal material as an analyte, since the milk is collected in a daily operation. However, the concentration of cortisol in the milk is lower than that in the blood [10–15]; it ranged from about 500 pg/mL to 10 ng/mL. In addition, many foreign substances are included in the milk. A detection system for cortisol requires high sensitivity with short detection time for livestock industry. We report primitive and positive data on stress monitoring for livestock industry.

Many methods were used for detecting cortisol in the milk. Radioimmunoassay (RIA) [10–12] and enzyme-linked immunosorbent assay (ELISA) [13–15] are well known as highly sensitive detection methods of cortisol. However, these techniques require time-consuming steps for secondary

Table 1: Surface treatment conditions and their properties of contact angle and the delta meaning frequency differences between Ch1 and Ch2 on the injection of 10 vol%-plain-milk-containing sample.

	1st reagent	2nd reagent	Contact angle [°]	Delta [Hz]
(a)	N102, 1/3	Not used	55	−44
(b)	IAS	Not used	61.4	36
(c)	Casein, 0.25 wt%	Not used	58.2	−10
(d)	Plain milk, 1/10	Not used	45	−20
(e)	N102, 1/3	Plain milk, 1/10	61.1	−2
(f)	N102, 1/3	Skimmed milk	57.3	−2.2
(g)	N102, 1/3	Casein, 0.25 wt%	58.8	−4

labeling and reactions. In addition, the handling of hazardous radioisotopes limits widespread use on RIA. We focused on quartz crystal microbalance (QCM) method, which is one of label-free and real-time measurement of antigen-antibody interaction with simplicity, convenience, and low cost [16–20]. Our group reported that QCM method could detect cortisol level ranging from 5 to 100 pg/mL [16]. However, no study has been published for detecting cortisol level in the milk using the QCM method. The major problem of the QCM method is the slightly large noise level caused by measurement environment, such as temperature and density of surrounding media. Since twin sensor removes these environmental influences, noise level can be decreased drastically [16, 17]. In this report, one channel was used as a reference (Ch1) and the other channel measured antigen-antibody interaction (Ch2). Difference of frequency shift between Ch2 and Ch1, delta, was corresponding to the amount of analyte bound on Ch2 without environmental influence. In addition, competitive assay was applied in this report, because the molecular weight of cortisol was too small to be detected directly on QCM. Sequential analysis system is desired for laboratory or cow-house use. Our sensing system is integrated with a flow injection analysis and the condition of regeneration was described in this paper. We reported primitive and positive data for stress monitoring using twin sensor QCM for the animal welfare.

2. Materials and Methods

2.1. Materials. Monoclonal antibody to cortisol (anti-Crt) was obtained from HyTest Ltd. (Turku, Finland). Cortisol 3-BSA (Crt-BSA) was purchased from Fitzgerald Industries International (MA, USA). Cortisol standard solution (500 ng/mL) was obtained from Cayman Chemical Company (MI, USA). Blocking reagent, N102, was from NOF Corporation (Tokyo, Japan). Immunoassay stabilizer (IAS) was from Advanced Biotechnologies Inc. (MD, USA). Phosphate-buffered saline (PBS, pH = 7.4), casein, sodium hydroxide, and glycine hydrochloride were obtained from Wako Pure Chemical Industries, Ltd. (Osaka, Japan). Plain milk including 2% milk fat was produced in Hokkaido (Japan) and purchased from a supermarket. Skimmed milk was obtained from Megmilk Snow Brand Co., Ltd. (Tokyo, Japan).

2.2. Coating of the Sensor Surfaces. The surface of the Au electrodes was treated using a preparation jig as follows. 170 μg/mL of anti-Crt was coated on Ch2 for 10 minutes firstly. After rinsing Ch2 with PBS, seven conditions of surface treatment were applied for Ch1 and Ch2 in the same way as shown in Table 1. The blocking reagents were prepared as below. N102 was diluted by 1/3 by adding PBS. IAS was used as it was. Plain milk was diluted by 1/10 by adding PBS. 1.1 mg of skimmed milk was dissolved in PBS. After casein was dissolved in 10 mM NaOH solution, concentration of casein was adjusted to 0.25 wt% by adding PBS. First, reagents were dropped on each sensor surface for 25 minutes. After rinsing with PBS, second reagents were dropped for 5 minutes. Here, (a), (b), (c), and (d) did not use secondary reagents. Finally, PBS was dropped on each sensor for 10 minutes and the surface was rinsed by PBS.

2.3. Sensor System and Measurement. Cortisol was detected using a NAPiCOS QCM system consisting of a thermostatic chamber and a frequency counter (Nihon Dempa Kogyo Co., Ltd.). Figure 1 shows the schematic figure of the QCM system integrated with a flow injection system and the twin sensor chip (inset). A micro syringe pump (Model 100, KD Scientific, MA, USA) and a sample injector (injection volume: 20 μL, 7125, Rheodyne, WA, USA) were connected to a micro flow cell (inner volume: 5 μL) in the QCM system through PEEK tubes. A 30 MHz twin sensor chip (PSA-E-3002T, Nihon Dempa Kogyo Co., Ltd.) had two Au electrodes, and each surface area of them was 7.75 mm^2. PBS was used as a carrier solution. The prepared sensor chip was connected with a micro flow cell, and the assembled cell was set in the thermostatic chamber and kept at 25°C. Sample solution was injected and frequency shifts on each channel were observed. Then, delta measurement (delta = Ch2−Ch1) was performed at the flow rate of 6 μL/min.

3. Results and Discussion

3.1. Sensing System. The basic principle of QCM sensor depends on the frequency shift by analyte adsorbed on the QCM resonator. The amount of the analyte adsorbed on the

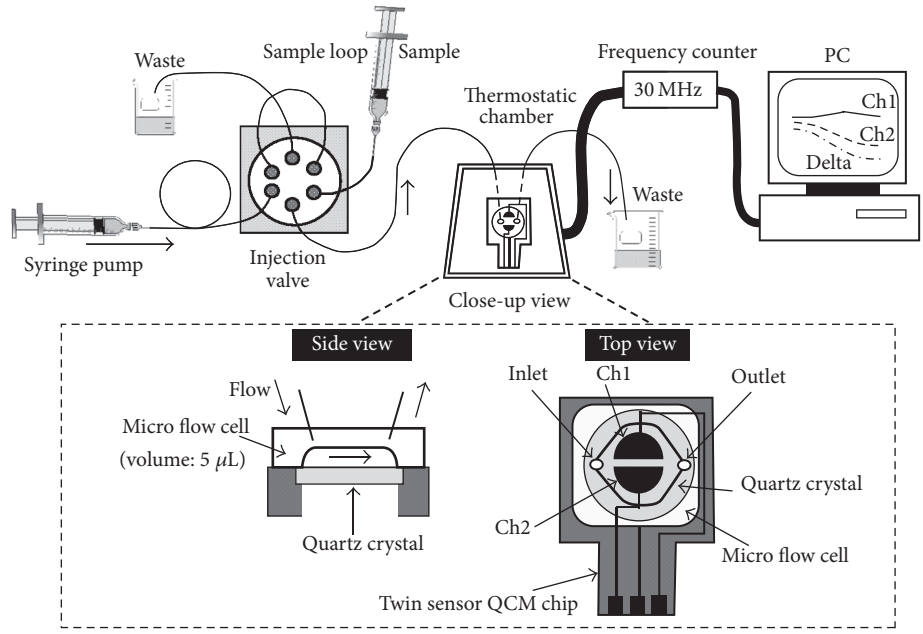

Figure 1: Schematic figure of our sensing system and the twin sensor chip on the QCM method.

QCM sensor can be determined using the following equation suggested by Sauerbrey [21]:

$$\Delta m = -\Delta F \times \frac{S \times \sqrt{\rho \times \mu}}{2N{F_0}^2}, \quad (1)$$

where Δm is the mass change corresponding to adsorption on the active electrode surface. ΔF is the change in the oscillation frequency of a quartz crystal. S, ρ, μ, N, and F_0 are the surface area of the electrode, the density of the quartz (2.65 g/cm^3), the quartz shear modulus (2.95×10^{11} g/cm·sec^2), the order of the overtone ($N = 1$ in this case), and oscillation frequency (30.8 MHz), respectively. Using the equation, theoretical mass change of the system was estimated to be 35 pg of analyte with the frequency shift of 1 Hz. Our QCM system used twin sensor and the delta between the frequency shifts on Ch1 and Ch2 was monitored. The delta remained lower than 1 Hz for 7 minutes, indicating that the sensing system achieved low noise level.

3.2. Delta Measurement of Milk Sample Corresponding to Surface Treatment. The surface of the sensor was very important to reduce the nonspecific adsorption of foreign substances in the milk. When the nonspecific adsorption occurs, it is acceptable that frequency shift of each channel performed similarly because of the delta measurement. Table 1 shows contact angle and the frequency difference between Ch1 and Ch2 (delta = Ch2 − Ch1) on seven surface coating conditions after a sample injection. Here, the sample contained 10 vol% of plain milk dissolved in PBS. Contact angle was measured using PX-G (Fibro System AB, Sweden) and that of bare Au was 83.2°. After the coating, contact angle degreased drastically but there were no characteristic properties corresponding to coating reagents. Bovine serum albumin (BSA) was known as a famous blocking material. We used IAS, which included BSA, at the beginning of the study. However, IAS did not reduce the nonspecific adsorption. Frequency change of each channel reached over 600 Hz, and delta was about 100 Hz after the sample injection. Milk contains casein as main protein, which accounts for nearly 80% of the milk protein. So, casein might adsorb on the sensor surface mainly. Casein contents of (c), (e), (f), and (g) were approximately the same. However, coating casein was not enough to reduce the nonspecific adsorption. Frequency change of each channel was about 100 Hz. Delta decreased to be −10 Hz but more effective coating was required. Blocking reagent of N102 consists of artificial macromolecule and does not include any proteins of animal origin. Only N102 coating did not show satisfying properties of the blocking for the sample including plain milk. Delta was about −44 Hz. Finally, we found the surface coating method suited for the sample. In fact, N102 was coated firstly, and the blocking buffer including casein was coated secondly. Using the above condition (e, f, g), delta was recorded to be lower than 4 Hz. For example, frequency shift corresponding to sample injection on the condition of (e) was shown in Figure 2. After the injection, frequency shift of each channel decreased because of nonspecific adsorption and viscosity changed corresponding to the sample. The frequency shift gradually increased and stayed at −55 Hz after the sample solution was replaced with the buffer. However, the delta showed about 2 Hz at the same time. The results indicated that the sensing system using the delta did not require any offset for cortisol detection in the milk.

Surface morphology was monitored by using AFM (SPI3800, SII NanoTechnology, Japan). Figure 3 shows AFM images of prepared sensor surface scanned over 2 μm × 2 μm with the tapping mode. Au surface on the sensor had a flat surface with Ra (average roughness) of 2.53 nm. After coating

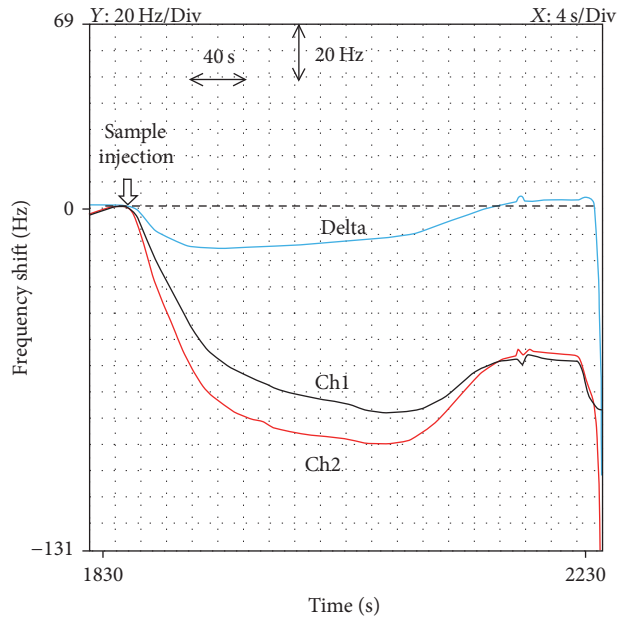

Figure 2: QCM responses on the sample injection. The sample contained 10 vol% of plain milk dissolved in PBS. The surface treatment of (e) in Table 1 was applied.

anti-Crt, surface morphology changed drastically. Antibody covered the Au surface as a whole. Surface morphology changed slightly corresponding to coating steps. Ra of prepared sensor was 2.76 nm after coating each reagent, which was almost the same as bare Au. The result indicated that the coating layer was very thin.

3.3. Sequential Analysis of the Sample. Flow injection analysis is suitable to examine a lot of samples. Sequential analysis system is desired for laboratory use. Uncoupling of the antibody-antigen interaction, called regeneration, was required for sequential measurements. Competitive assay was applied in this study, since the molecular weight of cortisol was 362, and the value was very small for the direct detection based on the QCM method. Sample solution including cortisol was injected with a constant concentration of tracer, which was a cortisol modified with a heavy substance. We used cortisol coupled with BSA (Crt-BSA) as the tracer because the anti-Crt had cross reactivity to the Crt-BSA. Molecular weight of BSA is 66 kDa, which is sufficiently large compared to that of cortisol. When the cortisol level was low, large frequency shift was observed, since the tracer bound to the anti-Crt mainly. On the other hand, when the cortisol level in the injected solution was higher, frequency shift was smaller, since a small amount of the tracer bound to the anti-Crt. Figure 4 shows an example of sample injection and regeneration process. The sample solution contained 10 vol% of plain milk and 2.5 μg/mL of the tracer. The frequency shif t on Ch1 shifted downward corresponding to the sample injection. This characteristic was due to the change of the viscosity of the sample solution. The frequency shift on Ch1 increased due to replacing the sample solution with the buffer. By contrast, the frequency shift on Ch2 decreased drastically. After reaching the lowest point, the frequency shift gradually increased until the sample solution was replaced with the buffer the same as Ch1. As a result, the delta stayed constant after the sample solution was completely replaced with the buffer. After the injection of 4 mM glycine-NaOH solution, the flow rate was changed to be 20 μL/min for 3 minutes for the regeneration. Then, the flow rate was set to be 6 μL/min again; the sensor response was reversed, since Crt-BSA deviated from anti-Crt. One determination cycle was within 10 minutes using our sensing system. As a result, we could detect the tracer without the influence of nonspecific adsorption and regenerate the QCM sensor a number of times.

To get a calibration curve, the sample solution was prepared as follows: the solution contained 10 vol% of plain milk and 2.5 μg/mL of the tracer with known concentration of cortisol. Calibration curve was obtained as shown in Figure 5. Error bars show the maximum and minimum values on each concentration ($N = 4$). The delta decreased with increasing the cortisol concentration from 0.1 to 100 pg/mL. It is noted that we did not consider the cortisol level included in the plain milk. The results show that our sensing system could determine the cortisol level of the milk, which was lower than 1 ng/mL.

4. Conclusions

We demonstrated a sequential detection method for a low molecular weight stress marker, cortisol in the milk, by using twin sensor QCM. Anti-Crt was coated on one channel (Ch2), and the blocking reagents were coated on both channels (Ch1 and Ch2) to reduce nonspecific adsorption. Ch1 was used as a reference. When the sensor surface was

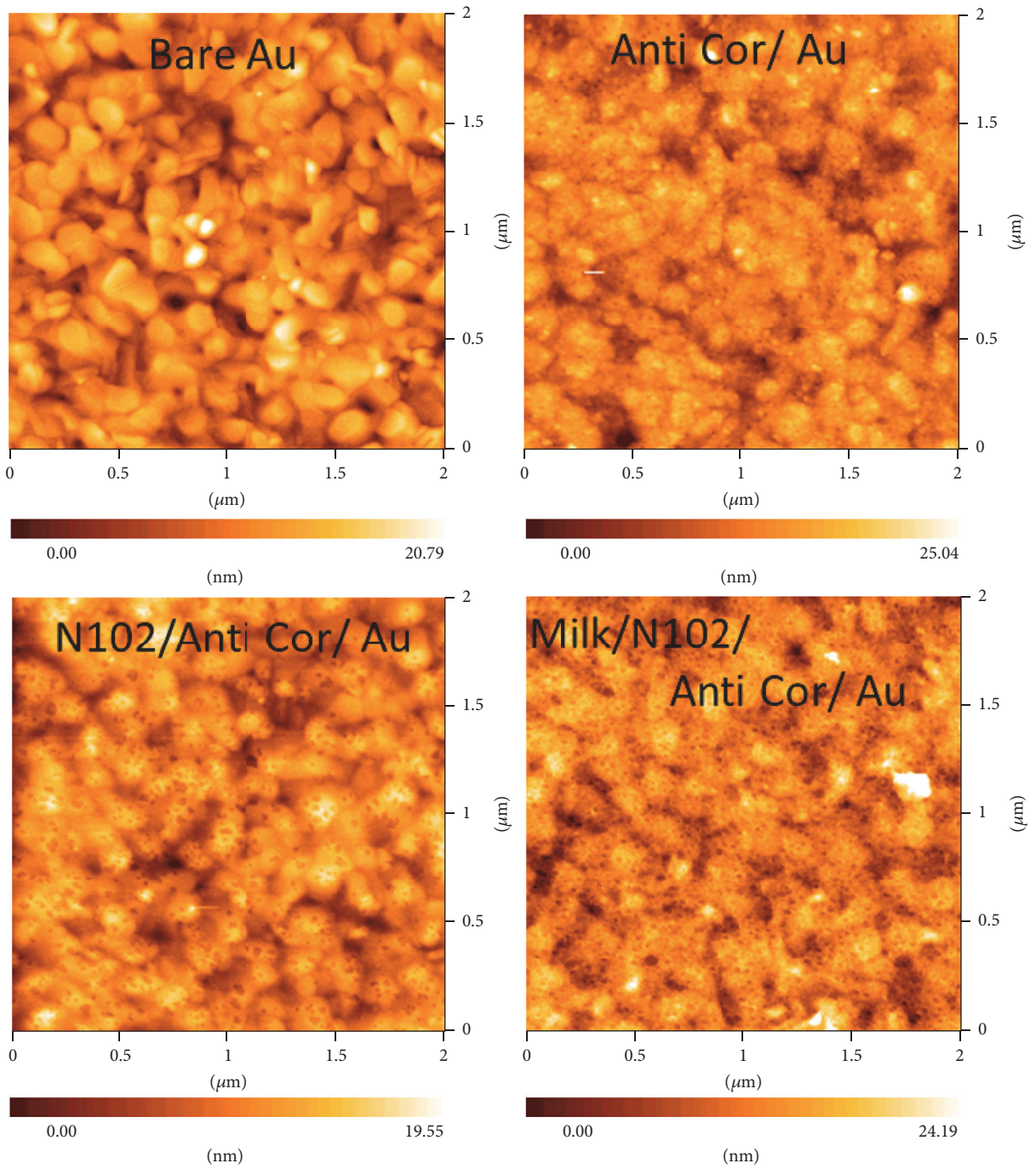

Figure 3: Surface morphology of some surface preparation by using tapping mode AFM. (a) Bare Au electrode. (b) Anti-Crt was coated on the Au electrode. (c) N102 was coated after the condition of (b). (d) The solution including 10 vol% of plain milk was coated after the condition of (c). Scan area was 2 μm × 2 μm.

optimized, the delta (Ch2 – Ch1) showed the real bonding amount without the nonspecific adsorption and environmental influences. It took 10 minutes for one determination cycle including regeneration of antigen-antibody interaction at the flow rate of 6 μL/min. The delta decreased with cortisol concentration from 0.1 to 100 pg/mL. These results indicated that our system using the twin sensor QCM showed high sensitivity and high throughput with repeatability.

Conflicts of Interest

The authors declare that they have no conflicts of interest.

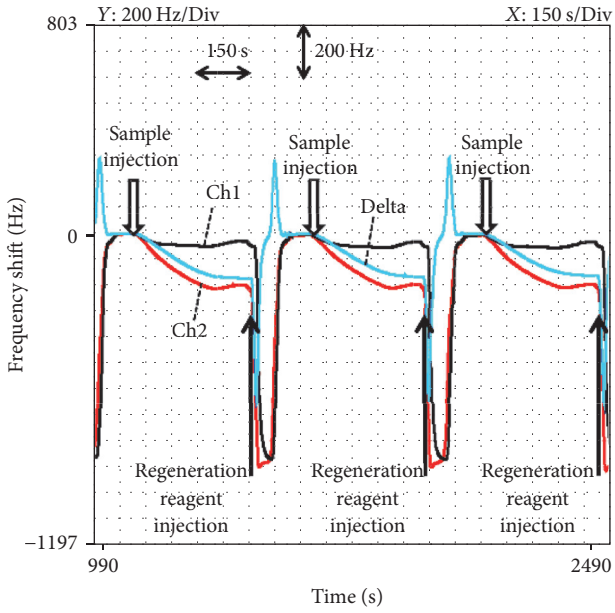

FIGURE 4: QCM responses on the sample injection and regeneration. The sample contained 10 vol% of plain milk and 2.5 μg/mL of the tracer (BSA coupled with cortisol) in PBS. 4 mM glycine-NaOH solution was used for the regeneration. The surface treatment of (e) in Table 1 was applied.

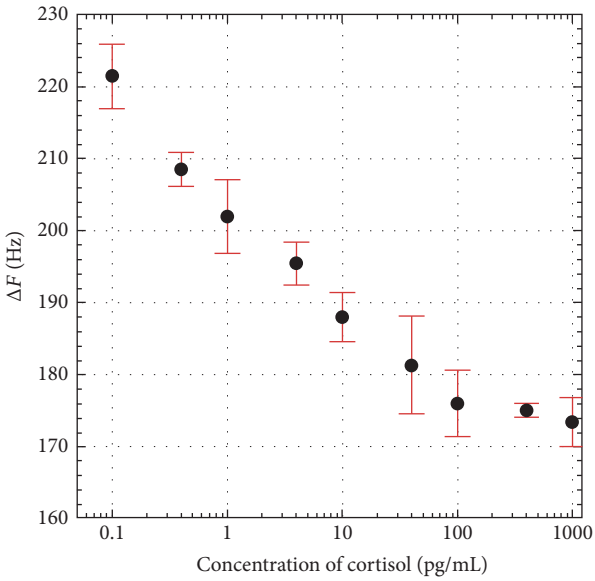

FIGURE 5: Calibration curve of cortisol on the sequential measurements. The condition of the sequential measurements was the same as that in Figure 4.

References

[1] M. Nagasawa, K. Mogi, and T. Kikusui, "Continued distress among abandoned dogs in fukushima," *Scientific Reports*, vol. 2, article 724, 2012.

[2] M. R. Kessler and D. C. Turner, "Stress and adaptation of cats (*Felis Silvestris Catus*) housed singly, in pairs and in groups in boarding catteries," *Animal Welfare*, vol. 6, no. 3, pp. 243–254, 1997.

[3] R. G. Beilharz and K. Zeeb, "Applied ethology and animal welfare," *Applied Animal Ethology*, vol. 7, no. 1, pp. 3–10, 1981.

[4] M. W. Fox, "Animal welfare and the dairy industry," *Journal of Dairy Science*, vol. 66, no. 10, pp. 2221–2225, 1983.

[5] J. L. Albright, "Status of Animal Welfare Awareness of Producers and Direction of Animal Welfare Research in the Future," *Journal of dairy science*, vol. 66, no. 10, pp. 2208–2220, 1983.

[6] B. A. Mallard, L. C. Wagter, M. J. Ireland, and J. C. M. Dekkers, "Effects of growth hormone, insulin-like growth factor-I, and cortisol on periparturient antibody response profiles of dairy cattle," *Veterinary Immunology and Immunopathology*, vol. 60, no. 1-2, pp. 61–76, 1997.

[7] F. Itoh, T. Komatsu, S. Kushibiki, and K. Hodate, "Effects of ghrelin injection on plasma concentrations of glucose, pancreatic hormones and cortisol in Holstein dairy cattle," *Comparative Biochemistry and Physiology - A Molecular and Integrative Physiology*, vol. 143, no. 1, pp. 97–102, 2006.

[8] Y. Saco, M. Fina, M. Giménez, R. Pato, J. Piedrafita, and A. Bassols, "Evaluation of serum cortisol, metabolic parameters, acute phase proteins and faecal corticosterone as indicators of stress in cows," *Veterinary Journal*, vol. 177, no. 3, pp. 439–441, 2008.

[9] D. J. Bristoe and D. S. Holmes, "Cortisol levels and anxiety-related behaviors in cattle," *Physiology & Behavior*, vol. 90, no. 4, pp. 626–628, 2007.

[10] W. R. Butler and C. K. Des Bordes, "Radioimmunoassay technique for measuring cortisol in milk," *Journal of Dairy Sience*, vol. 63, no. 3, pp. 474–477, 1980.

[11] S. B. Termeulen, W. R. Butler, and R. P. Natzke, "Rapidity of cortisol transfer between blood and milk following adrenocorticotropin injection," *Journal of Dairy Sience*, vol. 54, no. 11, pp. 2197–2200, 1981.

[12] C. Wenzel, S. Schönreiter-Fischer, and J. Unshelm, "Studies on step-kick behavior and stress of cows during milking in an automatic milking system," *Livestock Production Science*, vol. 83, no. 2-3, pp. 237–246, 2003.

[13] C. C. Cingi, D. F. Baser, Y. S. Karafakioglu, and A. F. Fidan, "Stress response in dairy cows related to rectal examination," *Acta Scientiae Veterinariae*, vol. 40, no. 3, article 1053, 2012.

[14] S. T. Long, N. C. Thinh, M. Yusuf, and T. Nakao, "Plasma Cortisol Concentrations after CIDR Insertion in Beef Cows," *Reproduction in Domestic Animals*, vol. 46, no. 1, pp. 181–184, 2011.

[15] M. Fukasawa, H. Tsukada, T. Kosako, and A. Yamada, "Effect of lactation stage, season and parity on milk cortisol concentration in Holstein cows," *Livestock Science*, vol. 113, no. 2-3, pp. 280–284, 2008.

[16] T. Ito, N. Aoki, S. Kaneko, and K. Suzuki, "Highly sensitive and rapid sequential cortisol detection using twin sensor QCM," *Analytical Methods*, vol. 6, no. 18, pp. 7469–7474, 2014.

[17] S. Kurosawa, JW. Park, H. Aizawa, S. Wakida, H. Tao, and K. Ishikawa, "Quartz crystal microbalance immunosensors for environmental monitoring," *Biosensors and Bioelectronics*, vol. 22, no. 4, pp. 473–481, 2006.

[18] L. Arce, M. Zougagh, C. Arce, A. Moreno, A. Ríos, and M. Valcárcel, "Self-assembled monolayer-based piezoelectric flow immunosensor for the determination of canine immunoglobulin," *Biosensors and Bioelectronics*, vol. 22, no. 12, pp. 3217–3223, 2007.

[19] C. March, J. J. Manclús, Y. Jiménez, A. Arnau, and A. Montoya, "A piezoelectric immunosensor for the determination of pesticide residues and metabolites in fruit juices," *Talanta*, vol. 78, no. 3, pp. 827–833, 2009.

[20] N. Mizutani, S. Korposh, R. Selyanchyn, S. Wakamatsu, and S.-W. Lee, "Application of a quartz crystal microbalance (QCM) twin sensor for selective label-free immunoassay to simultaneous antigen-antibody reactions," *Sensors and Transducers*, vol. 137, no. 2, pp. 1–9, 2012.

[21] G. Sauerbrey, "Verwendung von Schwingquarzen zur Wägung dünner Schichten und zur Mikrowägung," *Zeitschrift für Physik*, vol. 155, no. 2, pp. 206–222, 1959.

Hindawi
Journal of Sensors
Volume 2017, Article ID 8745437, 11 pages
https://doi.org/10.1155/2017/8745437

Research Article

An Innovative Serious Game for the Detection and Rehabilitation of Oral-Facial Malfunction in Children: A Pilot Study

Nuria Máximo-Bocanegra[1] and María-Luisa Martín-Ruiz[2]

[1]*Department of Physiotherapy, Occupational Therapy, Rehabilitation and Physical Medicine, Faculty of Health Sciences, Rey Juan Carlos University, Alcorcón, 28922 Madrid, Spain*
[2]*Department of Telematic and Electronic Engineering, Universidad Politécnica de Madrid, 28031 Madrid, Spain*

Correspondence should be addressed to María-Luisa Martín-Ruiz; marisam@diatel.upm.es

Received 30 January 2017; Revised 7 April 2017; Accepted 18 April 2017; Published 17 May 2017

Academic Editor: Guanghao Sun

We present SONRIE, a serious game based on virtual reality and comprising four games which act as tests where children must perform gestures in order to progress through several screens (raising eyebrows, kissing, blowing, and smiling). The aims of this pilot study were to evaluate the overall acceptance of the game and the capacity for detecting anomalies in motor execution and, lastly, to establish motor control benchmarks in orofacial muscles. For this purpose, tests were performed in school settings with 96 typically developing children aged between five and seven years. Regarding the different games, in the kissing game, children were able to execute the correct movement at six years of age and a precise movement at the age of seven years. Blowing actions required more maturity, starting from the age of five and achievable by the age of six years. The smiling game was performed correctly among all ages evaluated. The percentage of children who mastered this gesture with both precision and speed was progressively greater reaching more than 75% of values above 100 for children aged seven years. SONRIE was accepted enthusiastically among the population under study. In the future, SONRIE could be used as a tool for detecting difficulties regarding self-control and for influencing performance and the ability to produce fine-tuned facial movements.

1. Background

Currently, children are surrounded by technology, whether this being at home, at school, or in entertainment areas. Starting in kindergarten, at the age of five, children are beginning to learn via the use of technological gadgets such as iPads and computers [1]. Society today continuously introduces technology into as many aspects of life as possible, even at elementary schools, with the target of faster access to information, enhancing learning, and providing mechanisms for interaction that are motivating for children [2]. The book published in 1997 by Sandholtz et al. stated that "if technology is used appropriately, it has been shown to have many positive benefits and to create student-centered environments" [3]. Over recent years, after the appearance of the smart phone, it is especially striking to observe how children are interested in the use of technology at increasingly early ages and are able to learn to use these devices with comparative ease.

This paper presents SONRIE as a serious game based on virtual reality and which aims to facilitate the process of detection and rehabilitation of difficulties affecting the orofacial muscles in children aged between 4 and 12 years. A multidisciplinary team of professionals (comprising occupational therapists, physiotherapists, engineers, and child educators) designed and developed SONRIE using four games based on a medieval theme. SONRIE presents the child with tests (in the form of games) that require the execution of different facial movements which seek to detect the correct activation of the orofacial muscles during the performance of the same. SONRIE uses the 360 Kinect sensor and is based on virtual reality (VR) games; thus it is a low-cost solution.

Recently, the researchers involved in the design and development of SONRIE presented a study on the application of SONRIE to a group of 10 children with cerebral palsy (CP) aged between 4 and 12 years [4].

The current paper presents the results of a pilot study performed using SONRIE on a group of 96 typically developing children, attending the Amanecer School (Madrid, Spain). The research team established the working hypothesis that SONRIE would be accepted by children with typical development within the context of their own school. Thus, as stated in the work published by Druin in 1999, it was important to include the participation of children for the development of technology designed to be used by children [5, 6]. SONRIE is well-suited to the context of schoolchildren as it is based on a game. Also, the chosen theme is appropriate for the intended age of the participants and the form of use is both novel and appealing.

2. Methods

2.1. Participants. A total of 96 children (of both sexes) participated in this pilot study. The age of participants ranged between five and seven years and they attended the Amanecer School in Madrid, Spain. The mean age of participants was 5.84 and the standard deviation was 0.65. The Amanecer School is a private center attended by middle-class schoolchildren (although this sociocultural aspect has no implication in the results obtained). Before commencing the process of validation at Amanecer School, we had to consider ethical issues related to an intervention with a highly vulnerable population. This study was approved by the Ethics Committee of the Rey Juan Carlos University. The trial was conducted in accordance with the Declaration of Helsinki, amended in 2013 by the 64th World Medical Association (WMA) General Assembly (October 2013, Fortaleza, Brazil) [7].

This study evaluates the appearance of any type of difficulty during the performance of the movements, as requested by the different game interfaces, as well as the existence of correlations between better game skills according to the age or the sex of users. Furthermore, this study aims to establish motor control milestones for the orofacial muscles involved in the requested movements (execution with precision and speed).

At the onset of the study, a test was performed with a group of five children aged four years and children over the age of eight. This revealed that the younger children were lacking the sufficient attentional capacity to enable them to play the proposed games independently. This meant that the results would be invalid. For this reason, we decided to exclude four-year-old children from the group of tests performed. Moreover, in the children over the age of eight (with typical development) the performance of the different movements almost always provided high scores. Therefore, we considered that this study, when performed on healthy children over the age of seven, would not be relevant for the purpose of this research.

2.2. SONRIE Serious Game. Figure 1 presents the features of SONRIE, which shows all the screenshots of the SONRIE game. The SONRIE serious game and its framework have been developed by a multidisciplinary team of professionals. The game's design has considered the experience gained by occupational therapists while working with children with special needs.

2.3. Description of the Interfaces Featured in the SONRIE Game. Play motivates children and makes them want to participate in a particular activity, as long as it is designed within the parameters regulating games. Additionally, if it is interactive and technological, its capacity to motivate children increases and adhesion to treatment improves.

Physical therapists working with children may configure the SONRIE game according to the needs and progress of each child in order to design an effective therapy intervention. To achieve this, the therapist must set up a series of specific configurations [4]. For instance, the therapist can configure the number of repetitions for each game and establish a time limit for games.

The results obtained by each respective child for each game provide valuable information; thus, SONRIE continuously stores information regarding the performance of each child during the game, with data concerning whether the child has performed the movement or not, the time it took, and whether the child needed to use other muscles in order to accomplish the movement.

Thus, the gaming platform works by executing the stored values associated with each child and ensuring an appropriate and dynamic game. Once the game is over, the results are stored for subsequent review by a therapist.

The SONRIE's games cover each of the movements in a simple, guided way, using a motivating interface for the child.

When the game begins, the introductory screen appears (shown in Figure 2); next, the Kinect performs full-body skeleton detection and tracking. Subsequently, the eyebrow raising game begins.

This game runs until movement is detected or until the time limit for execution of the exercise has been reached. Figure 2 shows the start and end interfaces of the eyebrow raising and blowing games. As shown in Figure 2, we designed stimulating starting and ending screens for the children for each of the games.

If this screen is still on display after the half time limit, because the child has not yet performed the movement, an audible sound will be heard to provide the child with positive reinforcement (see Figure 2).

Once the gesture is considered appropriate, the number of times the game has been played is counted. If it is the first or second time, the eyebrow video will repeat, but if the count is higher, the program will continue to the next game. In other words, each game must be played the same number of times as the assessed repetitions, with a time limit that comes with each corresponding exercise [4].

The kissing and the smiling games follow the same procedures as the previous one: a wait until the movement

Figure 1: Interactive screens featured in SONRIE showcasing different games used to motivate children.

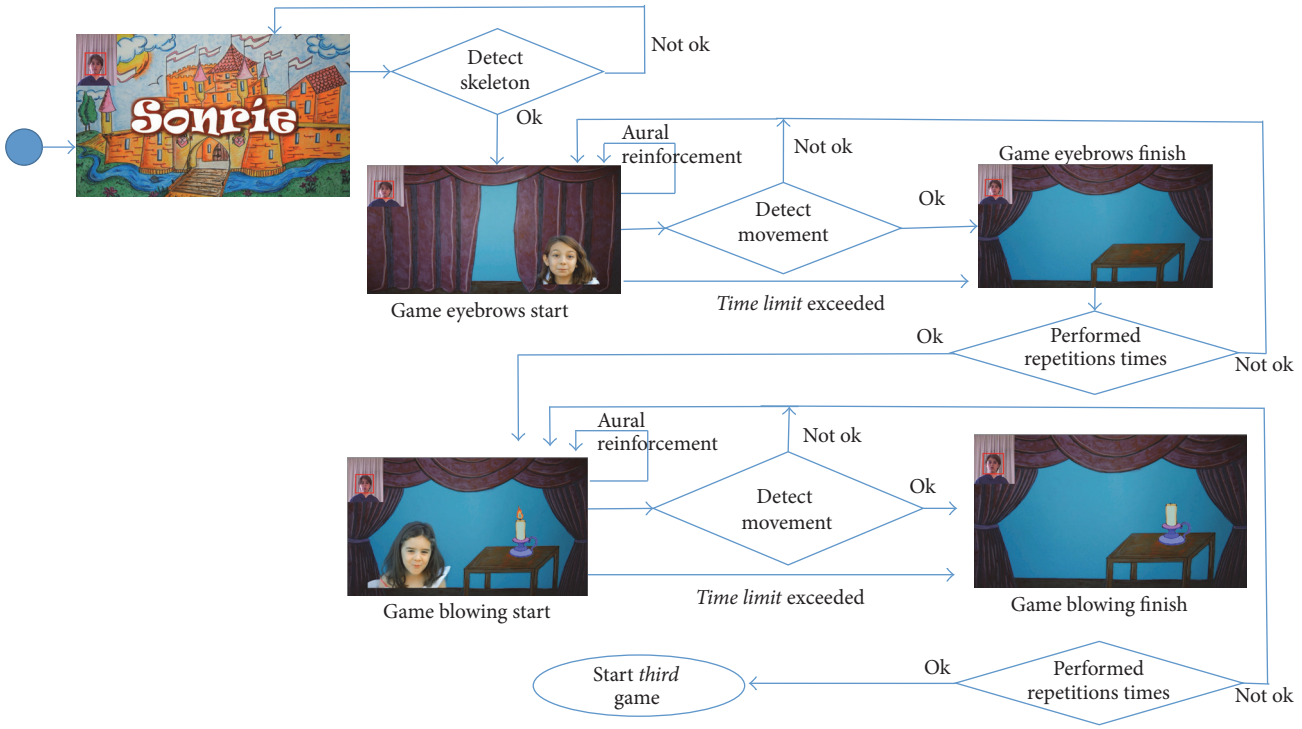

Figure 2: Activity diagram: start game, eyebrows rise, and blowing games.

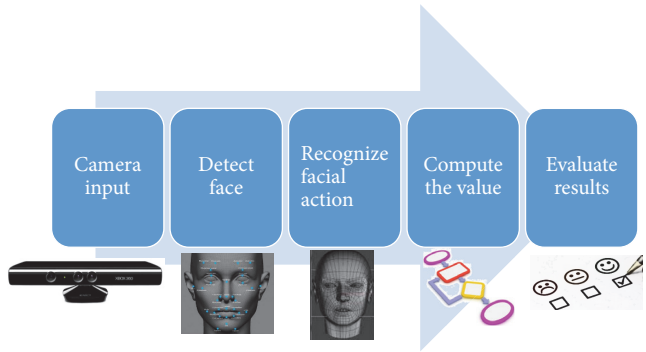

Figure 3: Stages necessary to carry out this study.

is recognized or the time limit is reached, which is followed by the final video for each game.

2.4. Description of the Values Returned by SONRIE

(i) Degree of acceptance: during the test with SONRIE in a real scenario, the children were asked about their satisfaction with the game after they played with the serious game. Up to 98.0% of children responded positively, showing great enthusiasm and acceptance towards the SONRIE serious game.

(ii) Accuracy and speed of movement: with the Kinect 360 sensor it is possible to measure the *accuracy of the requested movements*. This has been done for each of the movements by comparing the distances between the points involved in each movement before, and after, the execution of the same. This difference between distances enables the calculation of a threshold value that indicates the movement accuracy. Besides, the *speed of movement* is obtained as the difference between the time when the child is requested to perform the movement and the exact moment that the movement takes place.

(iii) Description of the algorithm used: during the execution of each game featured in SONRIE, the child obtains a numerical value (between −1 and 400) per game. This number indicates the precision and the execution speed of the child's facial movement as prompted by SONRIE.

Some possible values for the facial recognition algorithm are as follows:

(a) Negative values: the child performs the opposite movement to that proposed by SONRIE.

(b) Values between 0 and 99: the child executes a correct facial movement; nevertheless he/she does not reach the minimum threshold which measures the precision of the facial movement performed.

(c) Values between 100 and 400: the child successfully carries out the facial movement prompted by the SONRIE serious game. The return value increases depending on the seconds required and the precision of the facial movement.

2.5. Stages Carried Out in This Study. Figure 3 shows the main stages carried out by SONRIE serious game and the final study necessary in order to evaluate the results.

2.6. Occupational Performance in Children. The performance components constitute the skills needed to achieve each task. Without these, daily activities cannot be carried out effectively. These components [8], which may be classified into sensorimotor, cognitive, psychosocial, and psychological components, are strongly influenced by the context. Aspects such as the age of development, the chronological age, the health status, or the moment in the life cycle clearly influence the acquisition and successful engagement with each component.

Fisher et al. (2006) defined these skills as being small and measurable units in a chain of observed actions that occur while the person performs meaningful tasks [9]. These skills are learnt and developed over time and take place in specific contexts and environments. Rogers and Holm (2008) proposed that, during the development of these concrete skills during a task, several functions and structures of the body are united in unique combinations that may affect performance in daily life [10]. Therefore, no mathematical law or other law can be established to regulate the appearance of one or another isolated ability within the framework of each individual's behavior. To better understand this, we propose the graph featured in Figure 4, featuring a scenario where a child is asked to say her name in class when prompted to do so by a teacher.

During the game, in order for the child's occupational performance to be considered appropriate, two requirements must be initially fulfilled: these are *motivation* and *suitability* of the proposed activity according to the preferences and interests of the child [6]. When these requirements are fulfilled and considering the activity analysis of the components of performance proposed by Máximo-Bocanegra in 2011 [11], different and varied components are required which are gathered in Figure 5. SONRIE favors the practice

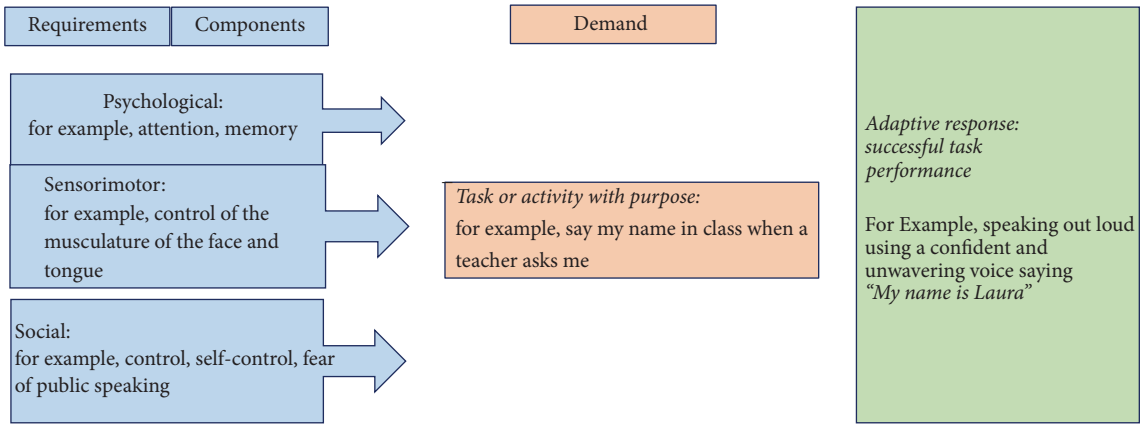

Figure 4: Performance components: activity analysis.

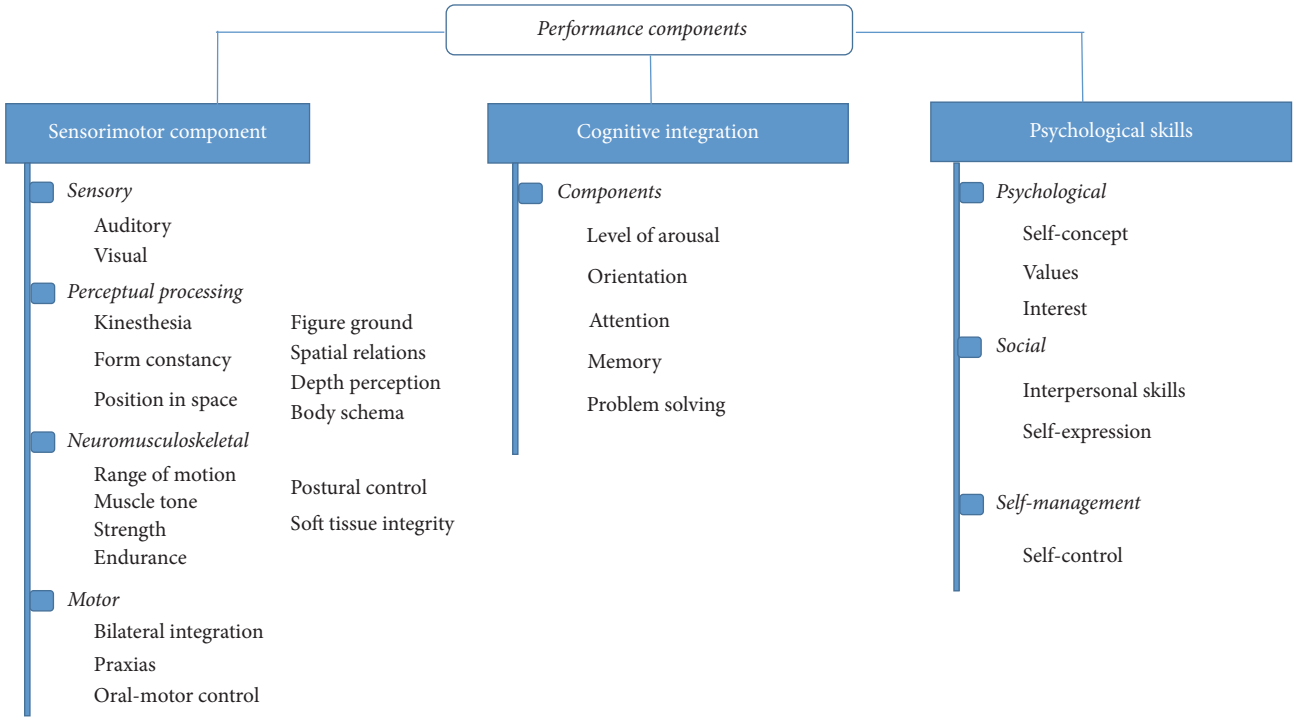

Figure 5: Performance components: analysis of activity.

of the following performance components: visual, muscle tone, praxis, oral-motor control, attention, self-expression, and self-control.

Regarding the sensorimotor component, the SONRIE sensor is able to detect changes that occur during the movement of certain muscles. Table 1 lists the facial muscles involved in each of the movements performed in SONRIE.

2.7. Statistical Analysis. To carry out the statistical analysis we decided to use a box and whisker plot, as these diagrams are one of the most commonly used in statistical analysis and are appropriate for the purpose of this study.

A box and whisker plot is especially useful for indicating whether a distribution is skewed and whether there are potential unusual observations (outliers) in the data set. Box and whisker plots are also very useful when large numbers of observations are involved and when two or more data sets are being compared, as applies to this experimental study.

A box and whisker plot is a way of summarizing a set of data measured on an interval scale. These diagrams are often

Table 1: Facial muscles involved in SONRIE.

Movement	Muscles involved
Kissing	Orbicularis oris
Blowing	Buccinator, orbicularis oris
Lifting eyebrows	Frontalis, corrugator supercilii, and upper eyelid orbicularis oculi
Smiling	Risorius, zygomaticus major, zygomaticus minor, caninus, levator labii superioris, and orbicularis oris

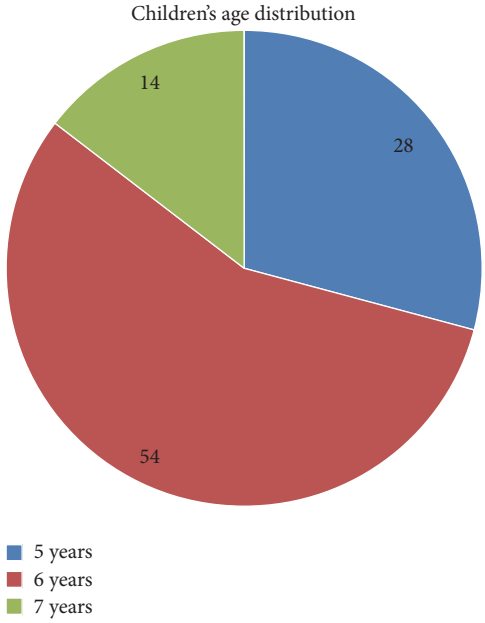

Figure 6: Age distribution of participating children.

used in explanatory data analysis by showing the shape of the distribution, its central value, and its variability.

3. Results

This study was performed over five sessions. Figure 6 represents the distribution of the sample by age. The most frequent age of participating children was six years. The age of participants is related to the fact that the tests took place in the month of May, and therefore many children in their final year of nursery school had already reached the age of six. Likewise, many first-grade students still had not reached seven years of age. The mean age of children participating in this study was 5.8 years.

One of the first objectives of the present pilot study was to analyze the acceptance of the game in children with typical development within the aforementioned ages. All the children who were invited to play with SONRIE were subsequently interviewed using an unstructured survey regarding their experience with the game. They were asked whether they liked it and whether they wanted to play again.

Table 2: Examples of results provided by SONRIE.

Result	Raising eyebrows	Blowing	Kissing	Smiling
Mean	*96,6*	*84,3*	*96,7*	*84,6*
Standard deviation	*120,6*	*48,9*	*120,6*	*227,75*

Up to 98.9% of children responded positively, showing great enthusiasm and acceptance towards SONRIE.

Regarding the objective of detecting possible execution anomalies, we were able to observe that 3% of the children under study displayed difficulties following the proposed games, as they were unable to remain still and attentive during the instructions provided, which resulted in subsequent execution errors. The researchers informed the school's educational psychology team of these results to enable them to evaluate the students and establish a follow-up process, if necessary.

On the other hand, this study aimed to evaluate whether differences existed in the execution of the movements evaluated in SONRIE and whether motor control milestones for the orofacial muscles could be established. To exemplify this, Table 2 displays the mean and the standard deviation provided by SONRIE for each game.

During the tests, observations of the children were made which were gathered in a register designed for this purpose. These observations helped clarify some of the difficulties displayed by the children. In the eyebrow raising game, 9% of the cases with a threshold of zero did not know how to raise their eyebrows and 2% were unable to stay still. In the smiling game, 1% moved a lot during the execution of the game. In one of the cases, a girl did not score well on the smiling game as she only raised one side of her mouth.

For the overall data analysis, we designed a graph with the complete data. Figure 7 graphically presents the distribution of the execution values for each of the games.

An analysis of the results shows that, in the first place, in the *smiling game (purple)* some data is above the threshold of 400. These values reflect an incorrect execution of the movement, as previously mentioned: that is, the researchers observed that these were children who were unable to stay still without moving other parts of the body. Due to the sensitivity of Kinect, if the child moves too much, the game produces values above 400 (indicative of a possible error).

On the other hand, analyzing the results based on the tests included in the four games, we can conclude that the behavior of the *blowing (red)* and *kissing* games *(green)* was similar with regard to the distribution of the data. During the performance of these games, most participants obtained performance threshold values between the first quartile (Q1) and the second quartile (Q2-median). This demonstrates that both these games are homogeneously sensitive in their relation with the developmental evolution of the child.

The game with the worst execution was that of *raising the eyebrows (blue)*, due to the fact that 51% of the time the game produced a threshold value of zero. However, this did not always mean that the child was unable to raise the eyebrows. This may be due to several reasons:

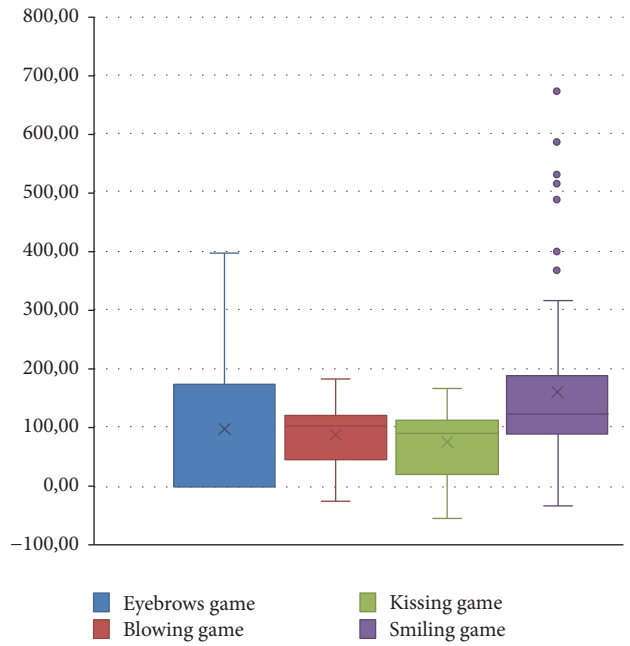

Figure 7: Box and whisker charts with the distribution of the results obtained for each of the games, according to the child's age.

(i) The child did not perform the movement with the necessary precision.

(ii) There may have been a lack of understanding of the movement required.

(iii) The order of the game in the series makes the execution more difficult, as the eyebrow raising game is the first movement that SONRIE displays.

(iv) The children have not yet automated the rules and content of the game.

Smiling is the game with the greatest dispersion of data. The inferior part of the box is greater than the superior half, as displayed in Figure 7. However, this does not necessarily mean that the thresholds returned by this game (between 25% and 50% of the sample) are more dispersed than those between 50% and 75%.

Figure 8 shows three box and whisker charts which establish the dispersion of the values obtained for each of the games, according to the child's age.

It is interesting to analyze the data obtained according to the age of the children. This analysis enables us to establish possible thresholds of motor control development for the orofacial muscles. The muscles involved in each movement are summarized in Table 1. Thus, in the kissing game (in green) a correct movement is obtained at the age of six, whereas a precise movement is obtained by seven years of age. Prior to these ages, the values are below 0, which is indicative of greater difficulties in the execution of this movement and, of course, a lack of precision.

For the blowing game, the data indicated that all children performed it correctly, without age distinctions; however, many five-year-old children obtained values below 100, whereas, after the age of six, approximately 75% of the values were above 100. This means that this movement is in the process of maturation from the age of five and is only attained by the age of six.

The smiling game was correctly executed among all the ages evaluated. The percentage of children who dominated the game with both precision and speed was progressively greater, reaching more than 75% of the values above 100, among the seven-year-old children.

The results of the eyebrow raising movement were similar among all age groups; the lowest value was 0 and there were some values registered above 300 among all age groups. However, as the number of six-year-old children was significantly higher (56% of the children were six years old) the median was 0, which indicated that a considerable number of children performed the correct movement without considering it to be precise and fast. This is due to the fact they only performed a slight eyebrow raising movement and failed to reach the minimum movement required.

Figure 9 graphically displays the median obtained by all the children in each game, grouped by age. We can see that, in all the games, except for the eyebrow raising game, an evolution of the motor execution of the requested movements took place. The seven-year-olds scored better than the six-year-olds, and these were better than the five-year-olds. Of the four games in SONRIE, the smiling game is where all children achieved the best execution. The eyebrow raising game is where there was the greater variability of data, showing a different tendency compared to that previously explained for the other games. There were no differences between values according to the participants' sex.

4. Discussion

Chen et al. [12] stated that the treatment of motor speech dysfunctions in children with CP requires an understanding of the mechanisms underlying motor control. However, there is a lack of literature on quantitative measures of motor control. The present findings, which are based on the SONRIE game, enable us to have a greater understanding of the oral-motor mechanisms underlying language, together with nonverbal communication and, even, the emotional expression of children without pathologies.

Games based on VR have been employed as therapeutic tools to circumvent possible difficulties in the rehabilitation set for children with CP, as well as for other neurological disorders [13, 14]. The last decade has produced many reports relating to the use of Kinect in processes of body rehabilitation, balance, motor control, upper limb rehabilitation, and even cognitive rehabilitation. Over the last year, several studies have been published focusing on the rehabilitation process or the detection of pathologies which affect the orofacial muscles in adults using VR. Among these, we can highlight the following: (1) studies based on healthy adults who present a prototype for the identification and scoring of asymmetries in facial palsy [15]; (2) also, a study proposing the creation of a database regarding facial expressions studied in people of different ethnicities aged between 7 and 80 years [16].

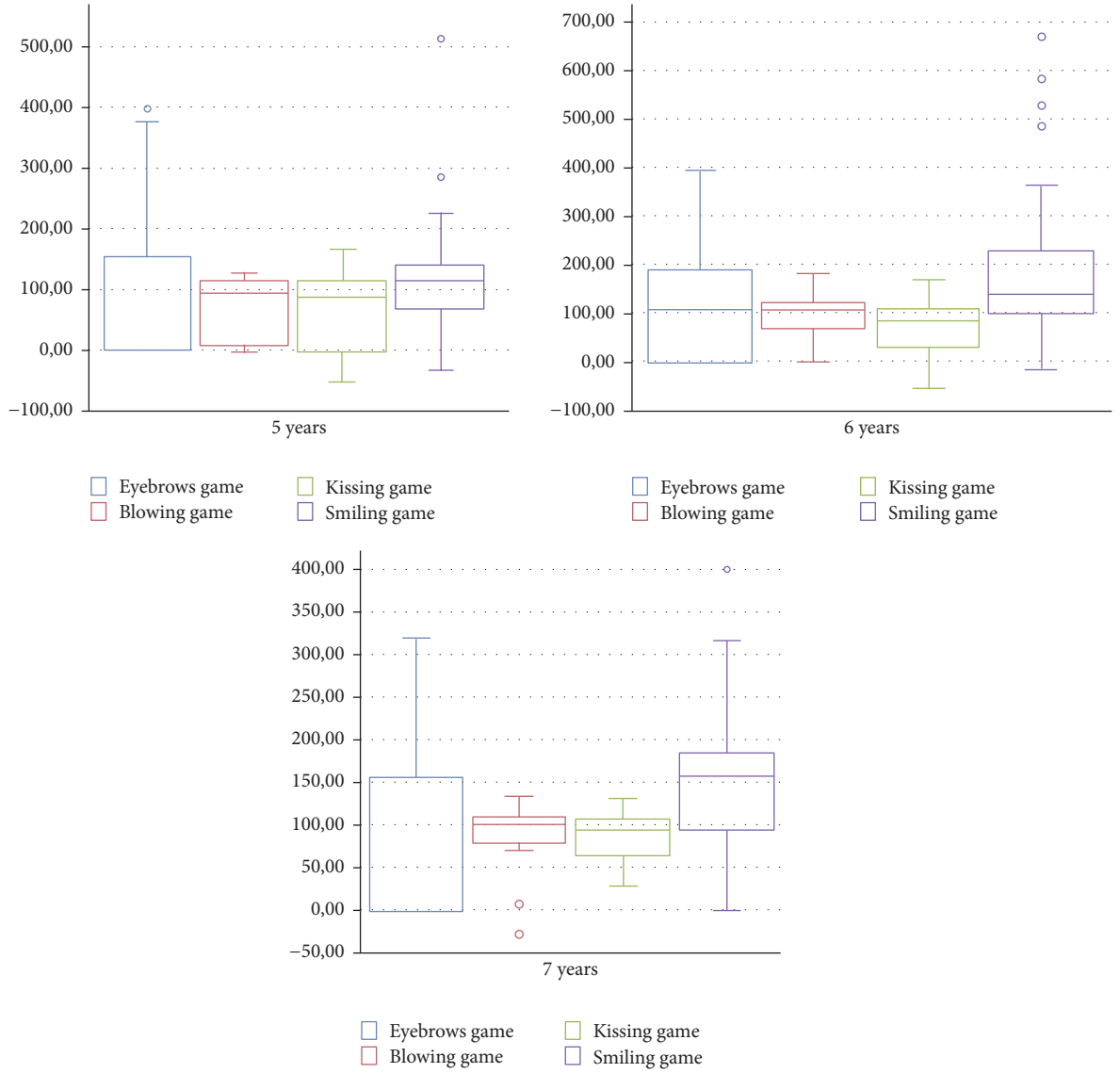

Figure 8: Distribution of the scores obtained for each of the games, according to the child's age.

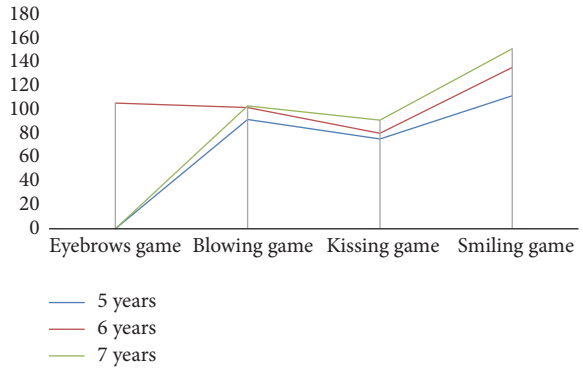

Figure 9: The resulting median for each game according to the children's age.

Table 3: Comparison of the related studies performed in adults and their outcomes.

Reference	Aim	Outcome
[13]	This study mapped different facial expressions in 150 subjects between 7 and 80 years of age of different ethnicities.	The purpose is to use them in various computer applications: facial image manipulation, face component transfer, real-time performance-based facial image animation, and facial animation retargeting from video to image.
[14]	This work aims at testing a cost-effective markerless approach for assessing kinematic parameters of hypokinetic dysarthria.	The results showed that Parkinsonian patients exhibit reduced peak velocity of the lower lip, during both the opening and the closing phase of the mouth. In addition, peak values of acceleration are reduced in Parkinsonian patients, although with significant differences only in the opening phase compared to healthy control subjects.
[12]	A comprehensive automated system to quantify and grade facial paralysis: resting symmetry assessment is grading the asymmetry of different regions of the face without any voluntary movement. The objective is to quantify the asymmetry between the left and right sides of the face for patients with facial paralysis as well as for normal controls.	Create a grading system for facial paralysis. The system is easy to use, of low cost, automated, and fast and is thus well suited for clinical use.

Furthermore, in support of our findings, the 19 expressions analyzed by Cao et al. include kissing, smiling, and raising the eyebrows [16]; lastly, (3) a study that was published using Kinect as a tool for the detection and rehabilitation of people with Parkinson's, which was considered as a highly valid tool due to its low cost and ease of use in the home [17]. It is difficult to compare studies with the same type of technology or similar to those that have been done, to date, among adults. The objectives and results of the studies found are very different from those established by SONRIE. Table 3 summarizes the relevant information concerning the studies performed to date on adults regarding the study of facial muscles.

One of the common aspects shared by SONRIE and these studies is the interest in the orofacial muscles. In addition, as a serious game, SONRIE fulfills several functions: it is a useful game among the population under study (completely unique providing data for use in the child population) and it may be used as a tool for the detection of possible motor disorders affecting the orofacial muscles, difficulties understanding instructions, attention difficulties, or lack of self-control in children [4]. We found that smiling is the game with the greatest dispersion of data. The explanation provided by the researchers is that smiling is the movement which allows the most variability in its execution, ranging from a small smirk to a broad smile. Furthermore, it depends closely on the expressiveness of each person, which explains the dispersion in the data.

Lastly, SONRIE is also a therapeutic tool which may be used to help detect cases or to help treat children with an established diagnosis affecting the functions and structures involved in this game. As reported by Gunel et al. in their study in 2014, VR provides new opportunities for rehabilitation professionals, even though these authors stress the need for further studies to be performed in order to prove its effectiveness [18]. In addition, it is worth noting that SONRIE is an educational tool as it grants an excellent opportunity to work on facial expressions in children as a way to improve their nonverbal communication and thus improve the expression of feelings and emotions and, as a result, enhance social relations.

The effect that learning has on the improvement of the motor execution of these muscles has already been demonstrated by some authors [19] and so this mechanism must be the basis of future projects using this tool. The study by Smith demonstrates the existing variability between children compared with adults in the execution of facial movements [19]. These differences, together with the previously mentioned learning factor, support the first explanation regarding the errors related to the eyebrow raising game: that is, as this is the first game, the children cannot rely on previous learning experience, which is further influenced by their condition as children. In future experiments, the order of the eyebrow raising exercise will be changed in order to verify whether this reduces the number of zeros obtained with its execution.

5. Conclusions

SONRIE is a valid tool for use in school contexts among a healthy population of children aged between five and seven years, which shows a high level of acceptance on behalf of the same.

Concerning the movements proposed by SONRIE, the eyebrow raising movement appears to be the most complex to perform with precision and speed for the age group under study. As commented previously, many thresholds were zero in the complete age range; therefore, this movement is not valid for measuring the maturity of the motor control of orofacial muscles. There is no evolution in the acquisition of precision and speed, but rather variability exists regarding the expressiveness of each child, as greater or lesser ranges of movement of the involved muscles were observed. Future

research will adapt the game settings in order to modify the position of the same in the series or by including a previous preparatory game to serve as a "demo" in order to improve the children's attention, learning, and, hence, performance.

On the other hand, the blowing and kissing movements displayed similar behavior regarding the sensitivity of the changes in the children's development. Smiling is the movement which is performed the earliest but also the one with the most subtleties during its execution.

Difficulties regarding self-control influence performance and the ability to produce fine-tuned movements. Therefore, in the future, SONRIE could be used as a tool for detecting these problems. For this purpose, subsequent studies should involve larger samples.

With Kinect 360, users with a fringe or wearing glasses may suffer from undermined scores due to problems related to the sensor. Future programs developed by SONRIE should use a more sophisticated sensor in order to avoid these problems, as is the case of Kinect 2.0.

Ethical Approval

The protocol was approved by the Local Ethical Committee of the Rey Juan Carlos University.

Consent

All participants signed informed consent for the use of all experimental data in scientific publications and in accordance with the policies about trials with human subjects before starting experimental and rehabilitation sessions.

Disclosure

Nuria Máximo-Bocanegra holds a Ph.D. degree at the University Rey Juan Carlos (2010) and a Master's degree in Neurological Pathologies. She is an occupational therapist and a specialist in early care. Nuria Máximo-Bocanegra is currently involved in several research projects in the field of occupational therapy for the improvement of children's occupational performance and participation. María-Luisa Martín-Ruiz received her Ph.D. from the Universidad Politécnica de Madrid (Spain) in 2014 and her Laurea (Graduate Diploma) Degree in Engineering Informatics in 2006 from the Universidad Carlos III, Madrid (Spain). Since December 2014, she is a Postdoc researcher in Telecommunications at the Universidad Politécnica de Madrid, where she is now an Assistant Professor in Telecommunications. At present, María-Luisa Martín-Ruiz works on intelligent systems, developing and validating the same for e-health and telemedicine scenarios. She is a Research Member of a research innovation group at the Universidad Politécnica de Madrid (T > SIC), in which she is working in applied research projects on AAL and home building automation, supported by regional and national funds.

Conflicts of Interest

The authors declare that they have no conflicts of interest.

Authors' Contributions

María-Luisa Martín-Ruiz and Nuria Máximo-Bocanegra have contributed equally to the manuscript.

Acknowledgments

The authors extend their gratitude to the professors and children from the Amanecer School for their participation in this study. Thanks are due also to Laura Luna, for her insightful help with the identification of the orofacial muscles targeted by the SONRIE program for the rehabilitation of children with cerebral palsy.

References

[1] A. Kersey, *The Role of Technology in Elementary Schools How has technology taken over? [PhD thesis]*, Indiana State University, 2016.

[2] J. C. Bartlett, "Teaching for tomorrow, today," *The Education Digest*, vol. 81, no. 6, pp. 4–8, 2016.

[3] J. Sandholtz, C. Ringstaff, and D. C. Dwyer, *Teaching with Technology: Creating Student-Centered Classrooms*, New York, NY, USA, 1997.

[4] M.-L. Martín-Ruiz, N. Máximo-Bocanegra, and L. Luna-Oliva, "A virtual environment to improve the detection of oral-facial malfunction in children with cerebral palsy," *Sensors*, vol. 16, no. 4, article 444, 2016.

[5] A. Druin, "Cooperative inquiry: developing new technologies for children with children," in *Proceedings of the SIGCHI Conference on Human Factors in Computing Systems*, pp. 592–599, ACM, Pittsburgh, Pa, USA, 1999.

[6] G. S. Moran, "Some functions of play and playfulness: a developmental perspective," *The Psychoanalytic Study of the Child*, vol. 42, pp. 11–29, 1987.

[7] World Medical Association, "World Medical Association Declaration of Helsinki," *The Journal of the American Medical Association*, vol. 310, no. 20, Article ID 2191, 2013.

[8] "Uniform terminology for occupational therapy," *American Journal of Occupational Therapy*, vol. 48, pp. 1047–1054, 1994.

[9] A. Fisher, "Overview of performance skills and client factors," in *Pedretti's Occupational Therapy: Practice Skills for Physical Dysfunction*, H. Pendelton and W. Schulz-Krohn, Eds., pp. 372–402, St. Lous Mosby/Elsevier, 2006.

[10] J. C. Rogers and M. B. Holm, "The occupational therapy process: evaluation and intervention," in *Willard and Spackman's Occupational Therapy*, Crepeau, E. S. Cohn, and B. A. B. Schell, Eds., pp. 650–657, Lippincott Williams & Wikins, Baltimore, Md, USA, 11th edition, 2008.

[11] N. Máximo-Bocanegra and M. Cigarán Méndez, "Análisis de la actividad," in *Gerontología y Geriatría: Valoración e Intervención*, J. C. Millán Calenti, Ed., pp. 171–186, Médica Panamericana, Madrid, Spain, Madrid edition, 2011.

[12] C.-L. Chen, H.-C. Chen, W.-H. Hong, F.-P. G. Yang, L.-Y. Yang, and C.-Y. Wu, "Oromotor variability in children with mild spastic cerebral palsy: a kinematic study of speech motor

control," *Journal of NeuroEngineering and Rehabilitation*, vol. 7, no. 1, Article ID 54, 2010.

[13] F. R. C. MacHado, P. P. Antunes, J. D. M. Souza, D. C. Levandowski, and A. A. D. Oliveira, "Virtual reality technology for rehabilitation of cerebral palsy: a literature review," *Trends in Psychology*, vol. 22, no. 3, pp. 565–577, 2014.

[14] I. Novak, S. Mcintyre, C. Morgan et al., "A systematic review of interventions for children with cerebral palsy: state of the evidence," *Developmental Medicine and Child Neurology*, vol. 55, no. 10, pp. 885–910, 2013.

[15] A. Gaber, M. F. Taher, and M. A. Wahed, "Quantifying facial paralysis using the kinect v2," in *Proceedings of the 37th Annual International Conference of the IEEE*, pp. 2497–2501, Milan, Italy, August 2015.

[16] C. Cao, Y. Weng, S. Zhou, Y. Tong, and K. Zhou, "Face warehouse: a 3D facial expression database for visual computing," *IEEE Transactions on Visualization and Computer Graphics*, vol. 20, no. 3, pp. 413–425, 2014.

[17] A. Bandini, S. Orlandi, F. Giovannelli et al., "Markerless analysis of articulatory movements in patients with parkinson's disease," *Journal of Voice*, vol. 30, no. 6, pp. 766.e1-766.e11, 2016.

[18] M. K. Gunel, O. K. Kara, C. Ozal, and D. Turker, "Virtual reality in rehabilitation of children with cerebral palsy," in *Cerebral Palsy-Challenges for the Future*, pp. 273–301, 2014.

[19] A. Smith, "Speech motor development: integrating muscles, movements, and linguistic units," *Journal of Communication Disorders*, vol. 39, no. 5, pp. 331–349, 2006.